THE JOURNAL OF PHYSICAL CHEMISTRY C
A JOURNAL OF THE AMERICAN CHEMICAL SOCIETY

pubs.acs.org/JPCC

Article

Exciting Opportunities for Solid-State ^{95}Mo NMR Studies of MoS_2 Nanostructures in Materials Research from a Low to an Ultrahigh Magnetic Field (35.2 T)

Hans J. Jakobsen,* Henrik Bildsøe, Martin Bondesgaard, Bo B. Iversen, Michael Brorson, Flemming H. Larsen, Zhehong Gan, and Ivan Hung

Cite This: *J. Phys. Chem. C* 2021, 125, 7824–7838

Read Online

ACCESS | Metrics & More | Article Recommendations | Supporting Information

ABSTRACT: Solid-state, natural-abundance ^{95}Mo NMR experiments of four different MoS_2 materials have been performed on a magnet at B_0 = 19.6 T and on a new series-connected hybrid magnet at 35.2 T. Employing two different 2H-MoS_2 (2H phase) materials, a "pseudo-amorphous" MoS_2 nanomaterial and a MoS_2 layer on an Al_2O_3 support of a hydrodesulfurization (HDS) catalyst, has enabled the introduction of solid-state ^{95}Mo NMR as an important analytical tool in the study of MoS_2 nanomaterials. ^{95}Mo spin−lattice relaxation time (T_1) studies of 160- and 4-layer 2H-MoS_2 samples at 19.6 and 35.2 T show their relaxation rate ($1/T_1$) increase in proportion to B_0^2. This is in accord with chemical shift anisotropy (CSA) relaxation, which is the dominant $T_1(^{95}Mo)$ mechanism, with a large ^{95}Mo CSA of 1025 ppm determined for all four MoS_2 nanomaterials. The dominant CSA mechanism suggests that the MoS_2 band gap electrons are delocalized throughout the lattice-layer structures, thereby acting as a fast modulation source ($\omega_o\tau_c \ll 1$) for ^{95}Mo CSA in 2H-MoS_2. A decrease in $T_1(^{95}Mo)$ is observed for an increase in the B_0 field and for a decrease in the number of 2H-MoS_2 layers. All four nanomaterials exhibit identical ^{95}Mo electric-field gradient (EFG) parameters. The T_1 results account for the several failures in retrieving the ^{95}Mo spectral EFG and CSA parameters for multilayer 2H-MoS_2 samples in the pioneering solid-state ^{95}Mo NMR studies performed during the past 2 decades (1990−2010) because of the extremely long $T_1(^{95}Mo)$ = ∼200−250 s observed at a low B_0 (∼9.4 T) used at that time. Much shorter $T_1(^{95}Mo)$ values are observed even at 19.6 T for the "pseudo-amorphous" and the HDS catalyst (MoS_2−Al_2O_3 support) MoS_2 nanomaterials. These allowed obtaining useful solid-state ^{95}Mo NMR spectra for these two samples at 19.6 T in a few to <24 h. Most importantly, this research led to the observation of an impressive ^{95}Mo MAS spectrum for an average of 1−4 layer thick MoS_2 on an Al_2O_3 support, that is, the first MAS NMR spectrum of a low-natural-abundance, low-γ quadrupole-nucleus species layered on a catalyst support. While a huge gain in NMR sensitivity, by a factor of ∼60, is observed for the ^{95}Mo MAS spectrum of the 160-layer sample at 35.2 T as compared to 14.1 T, the MAS spectrum of the 4-layer sample is almost completely wiped out at 35.2 T. This unusual observation for the 4-layer sample (crumpled, rose-like, and defective Mo-edge structures) is due to an increased distribution of the isotropic ^{95}Mo shifts in the ^{95}Mo MAS spectra at B_0 up to 35.2 T upon reduction of the number of sample layers.

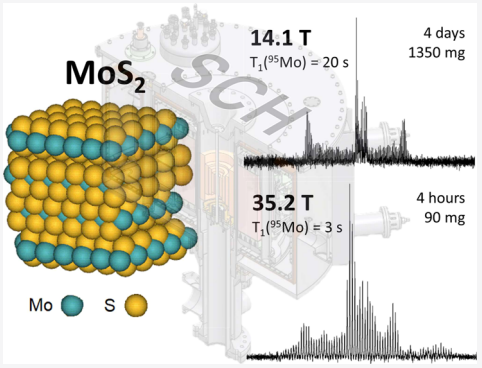

INTRODUCTION

The past decade has witnessed an enormous increase in the number of experimental and theoretical studies of the two-dimensional (2D) layered MoS_2 inorganic compound.[1] This material has for decades found general industrial applications as a lubricant because of its 2D layered (graphite-like) hexagonal 2H-MoS_2 crystal structure[2] and, most importantly, it has been used as the active component in heterogeneous hydrodesulfurization (HDS) catalysts worldwide at oil refineries.[3] The unusual revival in the high number of published MoS_2 scientific studies appears to be related to the advent of 2D graphene (general name for a one- or few-layer graphite carbon material),[4] which has received tremendous attention in research and industry because of the many potential applications of these 2D carbon-based materials, in particular, within the electronic industry. Thus, apparently, the astonishing properties observed for these graphene materials have triggered developments in related basic research areas for MoS_2 among chemists and physicists. For example, the synthesis and characterization of the corresponding single- or few-layered MoS_2 materials in order to understand their properties from both experimental and theoretical points of

Received: November 23, 2020
Revised: March 18, 2021
Published: April 1, 2021

view. For applications within catalysis (heterogeneous catalysis[5−7] and electrocatalysis[8]), the synthesis and characterization of such mono and few-layered MoS_2 materials have similarly been important research areas to enhance their catalytic activities.

With respect to the MoS_2 heterogeneous HDS catalysts, these catalysts usually consist of nano-sized MoS_2 particles dispersed on a high surface area γ-alumina (γ-Al_2O_3) and promoted by cobalt and nickel.[7] Today, the MoS_2−Al_2O_3 layered structures are particularly studied using transmission electron microscopy (TEM) or scanning TEM (STEM) techniques[9] developed during the past decades and combined with other analytical techniques such as chemical analysis, powder X-ray diffraction (PXRD), and optical spectroscopy methods.

The advent of natural-abundance solid-state ^{95}Mo (15.7%) NMR spectroscopy (static and MAS) of simple inorganic molybdenum compounds in 1990 resulted in the first determination of the anisotropic NMR parameters for this spin I = 5/2 quadrupole nucleus, that is, the ^{95}Mo quadrupole coupling (C_Q and η_Q) and chemical shift anisotropy (CSA) (δ_σ, η_σ, and δ_{iso}) parameters. These pioneering NMR studies, mainly initiated by Edwards and Ellis,[10] immediately paved the way for the almost 2 decades of struggle regarding solid-state ^{95}Mo NMR of MoS_2[10−14] before a precise and complete set of ^{95}Mo NMR parameters for a mineral multilayered sample of MoS_2 could be obtained in 2009, when a 14.1 T ^{95}Mo MAS spectrum of sufficiently high quality allowed these parameters to be extracted and published.[14] Three of these MoS_2 studies[10,11,13] used static ^{95}Mo NMR and one of these[11] also mentions two unsuccessful attempts to obtain a ^{95}Mo MAS spectrum, while the two remaining used MAS at higher magnetic fields of 19.6[12] and 14.1 T.[14] The main reason for the tremendous struggle with low-field (8.02−9.40 T) static experiments to obtain decent spectra is the long T_1(^{95}Mo) relaxation times for MoS_2, as quoted by these authors. For example, an unusually long recycle delay of 8 min (480 s) used at 9.4 T[11] and a T_1(^{95}Mo) = 255 s determined at 8.02 T[13] is quoted in these two studies. Similarly, a long T_1(^{95}Mo) is also experienced in the acquisition of the highly complex ^{95}Mo MAS spectrum at 14.1 T,[14] which required almost 4 days of spectrometer time, using a sample volume of 450 μL for a 7.5 mm o.d. rotor. In addition, because of the combination of a very large ^{95}Mo CSA, δ_σ = 1018 ppm, and C_Q(^{95}Mo) = 3.61 MHz, the highly complex appearance for the central transition (CT, +1/2< to >−1/2) in the −500 to −2300 ppm region of the ^{95}Mo MAS spectrum (shown in Figure 1) required consideration of the second-order cross-term[15−17] between the electric field gradient (EFG) and CSA tensors to obtain a perfect fit for the spectral simulation at 14.1 T. Thus, the combination of the above experimental difficulties and the high complexity of the acquired ^{95}Mo MAS spectrum is probably the main reason why, to our knowledge, no applications of solid-state ^{95}Mo NMR to MoS_2 in materials science have appeared during the past decade.

Since our 2010 communication,[14] we have been looking at various possibilities to further optimize the T_1(^{95}Mo)-dependent experimental conditions to obtain the ^{95}Mo MAS NMR spectra of mineral and synthetic samples of MoS_2. As mentioned earlier, our attention has been focused on the possibility to reduce T_1(^{95}Mo) at very high fields.[14] With the design, construction, and introduction of a series-connected hybrid (SCH) magnet in 2017[18] at the National High

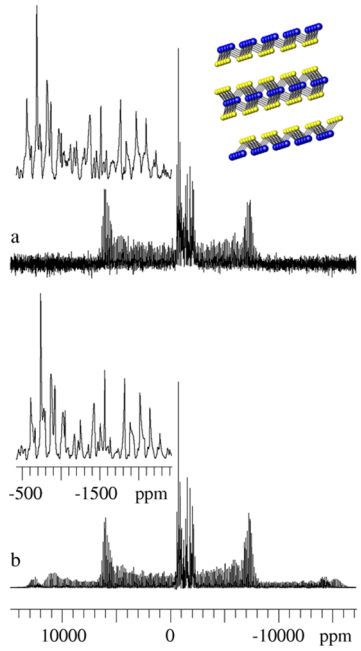

Figure 1. (a) Experimental 14.1 T (39.03 MHz) ^{95}Mo MAS NMR spectrum of the 160-layer MoS_2 exfoliated sample (sample 1), which allowed the first (and so far only) complete and precise set of solid-state ^{95}Mo NMR parameters for any kind of MoS_2 sample, ranging from a mineral to a standard MoS_2-surface catalytic sample, to be reported back in 2010.[14] This spectrum required almost 4 days of spectrometer time [82,000 transients with a 4 s relaxation delay (RD)] for the sample contained in a 7.5 mm o.d. rotor with a sample volume of 450 μL and for ν_r = 5.0 kHz (see the text for more details).[14] (b) Corresponding simulated spectrum using the optimized fitted parameters,[14] which are also listed in Table 1.

Magnetic Field Lab (NHMFL or MagLab), Tallahassee, Florida, and the construction of high-performance solid-state MAS NMR probes, such experiments became possible. As one of the first SCH magnet "users", a ^{95}Mo MAS NMR study on the same MoS_2 sample as used in the original experiment[14] was about the allocated spectrometer time in February 2018.

Preliminary experiments in February 2018 resulted in a ^{95}Mo MAS NMR spectrum for our original sample in less than 4.5 h and most importantly with a huge gain in sensitivity by a factor of about 60 compared to the original spectrum.[14] This gain includes consideration of almost all experimental parameters between the 14.1 and 35.2 T spectrometers (vide infra). The successful outcome of this first 35.2 T SCH ^{95}Mo MAS NMR experiment immediately triggered a number of questions to be investigated and answered in this research. A main question concerns the reason(s) for the unusually high gain in sensitivity observed at 35.2 T compared to 14.1 T. Is the apparent significant decrease in T_1(^{95}Mo) at a very high magnetic field caused by a contribution from (i) the large CSA (δ_σ = 1018 ppm)[14] or (ii) a possible reduction of the electronic band gap for the MoS_2 semiconductor at a high magnetic field, causing T_1(^{95}Mo) to decrease by release of additional electrons, or (iii) a combination of (i) and (ii)? Furthermore, in addition to the investigation at 35.2 T on the multilayered 2H-MoS_2 mineral sample, studied earlier at 14.1 T,[14] it has been of immediate interest to investigate if the solid-state ^{95}Mo NMR spectroscopy of three commonly encountered MoS_2 nanostructures in materials science (all in different crystalline states) exhibits a similar behavior with a change in magnetic

https://doi.org/10.1021/acs.jpcc.0c10522
J. Phys. Chem. C 2021, 125, 7824−7838

field. Thus, the present study explores the impact of magnetic field on the solid-state ^{95}Mo NMR spectra of MoS_2 nanoparticles (such as a "pseudo-amorphous" MoS_2 sample and a surface MoS_2-layer on an Al_2O_3 support) and nanostructure designs (e.g., a 160-layer vs a 4-layer MoS_2 sample). The results are intriguing, for example, the observation of a ^{95}Mo MAS spectrum for the surface MoS_2-layer on the Al_2O_3 support at 19.6 T is, to our knowledge, the first MAS NMR spectrum reported for a low-natural-abundance, low-γ quadrupole-nucleus species layered on a catalyst support. With the positive ^{95}Mo MAS NMR results obtained for the 160-layer sample (vide infra), a surprising observation is the near complete disappearance of the ^{95}Mo MAS spectrum for the 4-layer sample at 35.2 T. The explanation for this occurrence is revealed by using a combination of different solid-state NMR techniques, which appear particularly efficient as problem solvers in the elucidation of MoS_2 nanostructures by solid-state ^{95}Mo MAS and QCPMG[19−21] NMR.

Overall, the use of solid-state ^{95}Mo NMR methods to multi and a few-layered MoS_2 samples along with its applications to two different MoS_2 nanostructures at a high (19.6 T) and an ultrahigh magnetic field of 35.2 T at the NHMFL presented here for the 160- and 4-layer MoS_2 samples has provided a breakthrough and an exciting new tool for structural characterization of many MoS_2 nanostructures undergoing studies in materials science. For example, the $T_1(^{95}Mo)$ relaxation data, obtained in the present research, show that amorphous and catalyst MoS_2 samples are amenable to good NMR-sensitivity studies at low magnetic fields of 9.4−14.1 T, as opposed to multilayered MoS_2 samples. With solid-state NMR known to be sensitive to changes in the local environment of a nucleus, solid-state ^{95}Mo NMR techniques applied to MoS_2 have been now proven useful in providing local structural information for 2H-MoS_2 materials in a reasonable experiment time. Such information, as for example, the small isotropic ^{95}Mo chemical shift differences for the catalytic active ^{95}Mo edge-sites would be hard to obtain using other non-NMR tools such as PXRD, scanning tunneling microscopy (STM), or high-angle annular dark-field-STM. Examples of such new structural information obtained by solid-state ^{95}Mo NMR are obvious from the presented spectra, most of which are acquired within a time frame of 30 min to 48 h depending on the sample, that is, a remarkable time saving compared to our original study.[14] With some experience gained for the spectral outlook of a specific sample and the employed magnetic field strength, the spectra can often be used simply as benchmarks ("fingerprints") for the sample, in both a qualitative and a quantitative manner. Finally, for MoS_2 samples exhibiting sufficiently low $T_1(^{95}Mo)$ values, we estimate that low-field NMR spectrometers down to 9.4 T may be used to successfully perform some of the ^{95}Mo NMR experiments reported here in a reasonable time.

RESULTS AND DISCUSSION

The identity of the four MoS_2 samples investigated is as follows: sample 1 is a 160-layer MoS_2 sample obtained by exfoliation of a commercial mineral molybdenite sample. Sample 2 is a "pseudo"-amorphous sample produced at Haldor Topsøe (HT) A/S and sample 3 is a real MoS_2−Al_2O_3 catalyst sample produced by the HT group. Sample 4 is a 4-layer MoS_2 synthesized at Aarhus University.

Sample 1: MoS_2 160-Layer Exfoliated Sample. The successful recording of the ^{95}Mo MAS NMR spectrum for this sample at 35.2 T at the NHMFL in February 2018 triggered the present research aiming at a breakthrough in the application of solid-state ^{95}Mo NMR to MoS_2 in materials science. In the subsequent year, time at the 19.6 T and the new 35.2 T SCH facility were obtained in February 2019 at the MagLab. The experimental and optimized simulated MAS spectrum of sample 1 at 35.2 T, obtained using the same sample and identical experimental acquisition parameters as earlier,[14] is shown in Figure 2. The corresponding fitted spectral parameters are summarized in Table 1 along with those determined earlier at 14.1 T[14] for comparison. The two sets of spectral parameters are identical within the error limits for their respective experiments, despite the huge difference in the appearance of the two spectra. Some of the most surprising differences in the 14.1 T (Figure 1) and 35.2 T (Figure 2) ^{95}Mo MAS NMR spectra for sample 1 are summarized in Table 2.

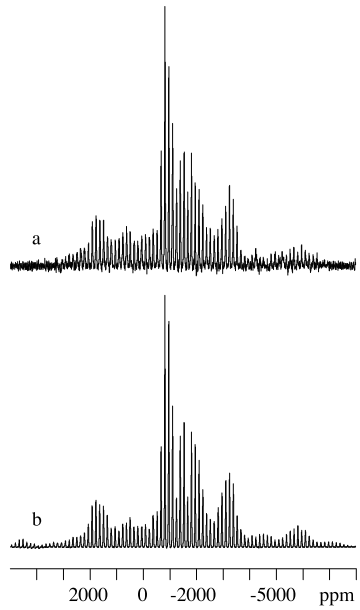

Figure 2. (a) Experimental 35.2 T (97.63 MHz) ^{95}Mo MAS NMR spectrum of the 160-layer MoS_2 exfoliated sample (sample 1). The spectrum was acquired using 4032 scans in 4.5 h with a RD of 4 s and for ν_r = 14.0 kHz. (b) Corresponding simulated spectrum (including the CT and the satellite transitions (STs) for both the two inner STs (±3/2< to >±1/2) and the two outer STs (±5/2< to >±3/2) for the I = 5/2 ^{95}Mo nucleus) and using the optimized fitted quadrupole coupling (C_Q) and chemical shift parameters (δ_σ and δ_{iso}) summarized in Table 1.

Thus, the above points contribute to the gain in sensitivity by a factor of ∼60, as estimated in the Introduction (vide supra), for the spectrum obtained at 35.2 T.

To understand the reason for the huge time saving in the acquisition for sample 1 at 35.2 T relative to 14.1 T, our attention has been focused on a useful method for the determination of $T_1(^{95}Mo)$ at the two available magnetic fields of 19.6 and 35.2 T in a reasonable time compared to the estimated $T_1(^{95}Mo)$ values of several 100 s experienced in the early studies at a much lower field.[10−14] Because of the general sensitivity gain obtained for the QCPMG experiment[19−21] in comparison to static and also MAS NMR, it was decided to use

https://doi.org/10.1021/acs.jpcc.0c10522
J. Phys. Chem. C 2021, 125, 7824−7838

Table 1. ^{95}Mo Quadrupole Coupling (C_Q and η_Q) and Chemical Shift Parameters (δ_σ, η_σ, and δ_{iso}) for MoS_2 in the Four Different Samples (Samples 1−4) Investigated in This Research and Determined from the ^{95}Mo MAS NMR Spectra at 19.6 and 35.2 T

MoS_2 in sample #/name	B_0 (T)	C_Q (MHz)	η_Q	δ_σ (ppm)	η_σ	δ_{iso} (ppm)	ψ, χ, ξ (deg)
#1/160-layer	14.1[a]	3.61	0.01	1018	0.00	−1231	[a], 1°,[a]
#1/160-layer	35.2[b]	3.61	0.10	1032	0.05	−1232	[b], 3°,[b]
#2/pseudo-amorph	19.6[b]	3.61	0.18	1030	0.03	−1234	[b], 2°,[b]
#3/Al_2O_3−MoS_2	19.6[c]	3.61[c]	0.18[c]	1030[c]	0.03[c]	−1234[c]	0[c], 0[c], 0[c]
#4/004-layer	19.6[c]	3.61[c]	0.18[c]	1030[c]	0.03[c]	−1234[c]	0[c], 0[c], 0[c]

[a]The solid-state ^{95}Mo NMR parameters determined for sample 1 at 14.1 T, reported earlier[14] and for the corresponding ^{95}Mo MAS spectra shown in Figure 1. The δ_{iso} values (determined indirectly relative to 2.0 M aqueous Na_2MoO_4; see the text) have an error limit of ±2 ppm. The error limits for C_Q, η_Q, δ_σ and η_σ are ±0.01 MHz, ±0.02, ±10 ppm and ±0.02, respectively. The Euler angles ψ and ξ that are undefined while $\chi = 1°$, resulting from an optimized fitting, has an error of ±8°, as determined at 14.1 T (ESI[14]). [b]Optimized fits and parameters for the spectra of sample 1 and sample 2 determined at 35.2 T and 19.6 T, respectively. The error limits for the η_Q and η_σ parameters are somewhat larger at the higher magnetic fields due to the increase in line broadening at 35.2 T (Figure 2) and 19.6 T (Figure 7) and are caused by the isotropic chemical shift dispersions in both samples (see the text). [c]Straightforward simulations (nonoptimized fits) of the^{95}Mo MAS NMR spectra presented in this research for sample 3 and sample 4 at 19.6 T. The simulations used the fixed parameter (label [c]) determined (Table 1, row 3) from the optimized fitted spectrum for sample 2 at 19.6 T (Figure 7b).

Table 2

reasons for the gain	14.1 T spectrometer	35.2 T spectrometer
	$\nu(^{95}Mo)$ = 39.03 MHz	$\nu(^{95}Mo)$ = 97.63 MHz
spectrometer time	3.8 days; 91 h	0.2 days; 4.5 h
		gain factor: 20
rotor size	7.5 mm o.d.	3.2 mm o.d.
sample volume	450 μL	30 μL
		gain factor: 15
spinning sideband line widths	250 Hz ∼ 6 ppm	1450 Hz ∼ 15 ppm
		gain factor 2 in S/N
spectral parameters	CSA: 1025 ppm ∼ 40 kHz	CSA: 1025 ppm ∼ 100 kHz
CSA - C_Q	C_Q: 3.61 MHz	C_Q: 3.61 MHz
	CT: high complexity	CT: low complexity
field dependence	highly complex, narrow CT with extensive line splitting caused by second order quadrupole broadening	CSA: displacement for part of CT to low frequency
CSA - C_Q		C_Q: reduced second order line broadening

the QCPMG pulse sequence with different recycle delays D1, that is, T_1QCPMG, as outlined in the Experimental Section. Figure 3 illustrates the series of six QCPMG spectra obtained at 19.6 T for sample 1 observed using RD D1 = 1, 3, 5, 7, 9, and 11 s. The spectra in Figure 3 were processed (see the figure caption) for optimized extraction of $T_1(^{95}Mo)$ from the peak heights, as described in the Experimental Section. Six different "spikelets" of the largest peak heights in the center for each of the six spectra (i.e., six D1-values) were selected for the optimized fitting to six different exponential curves. Figure 4 illustrates the resulting fits to the six exponential plots, which led to the following six slightly different $T_1(^{95}Mo)$ values: 10.3, 10.2, 11.6, 10.6, 10.6, and 12.2 s, giving an average $T_1(^{95}Mo)$ = 10.9 ± 1.6 s at 19.6 T. The six D1 values used in this T_1 experiment at 19.6 T are all lower or about equal to the six extracted $T_1(^{95}Mo)$ values shown above and the reason we consider $T_1(^{95}Mo)$ = 10.9 ± 1.6 s a lower limit. Performing the T_1QCPMG experiment for sample 1 at 35.2 T used RD D1 = 1, 3, 5, and 7 s and the five neighboring "spikelets" centered around the carrier-frequency "spikelet" were used in the exponential fits for $T_1(^{95}Mo)$. This resulted in a mean value $T_1(^{95}Mo)$ = 2.8 ± 0.4 s at 35.2 T. The two $T_1(^{95}Mo)$ values determined for sample 1 at 19.6 and 35.2 T are summarized in Table 3 along with the T_1QCPMG values determined for the three other samples.

The large decrease in $T_1(^{95}Mo)$ by a factor of ∼4 observed by an increase in magnetic field B_0 from 19.6 to 35.2 T is one of the significant reasons for the gain in sensitivity observed for the spectrum in Figure 2 compared to the result at 14.1 T.[14] This factor for $T_1(^{95}Mo)$ led us to consider the ^{95}Mo CSA (∼1025 ppm) as being the main relaxation mechanism for the MoS_2 160-layer in sample 1, as speculated on in the earlier study.[14] The general expression for the CSA relaxation rate $(1/T_1)$ is

$$(1/T_1)^{CSA} = (2/15)\gamma^2 B_0^2 \Delta_\sigma^2 \tau_c \quad (1)$$

where, for the present research on solid-state ^{95}Mo NMR in MoS_2, $\gamma = \gamma(^{95}Mo) = -1.7520 \times 10^7$ (rad T^{-1} s^{-1}), B_0 (T) is the magnetic field strength, $\Delta_\sigma = -(3/2)\delta_\sigma$, that is δ_σ = 1025 ppm, and τ_c is a ^{95}Mo correlation time, that is, the relaxation rate $(1/T_1)^{CSA}$ increases with the square of the magnetic field strength. Equation 1 is valid under the condition of $\omega_o\tau_c \ll 1$ (extreme motional narrowing regime), which is the case in solution, where $(1/T_1)^{CSA}$ is proportional to the size of the CSA interaction modulated by the molecular tumbling. In solids, such tumbling is absent and it is the modulation of the CSA interaction by lattice motions that matters. Such a lattice motion is often named "phonon" in NMR and electron paramagnetic resonance relaxation studies of frozen samples.[11,13,22] From our field-dependent $T_1(^{95}Mo)$ measurements for the 2H-MoS_2-layered samples, it is apparent that modulation of the CSA is much higher than for the EFG interaction. Therefore, the experimental results suggest that the semiconductor 2H-MoS_2 band gap electrons are the likely modulation-source for the ^{95}Mo CSA, in the sense that these electrons are delocalized throughout the lattice, similar to the conducting electrons in a metal. In the latter case, the conducting electrons induce a large field-proportional Knight shift, but little effect on the EFG. Thus, our field-dependent results indicate that ^{95}Mo CSA relaxation in addition to

https://doi.org/10.1021/acs.jpcc.0c10522
J. Phys. Chem. C 2021, 125, 7824−7838

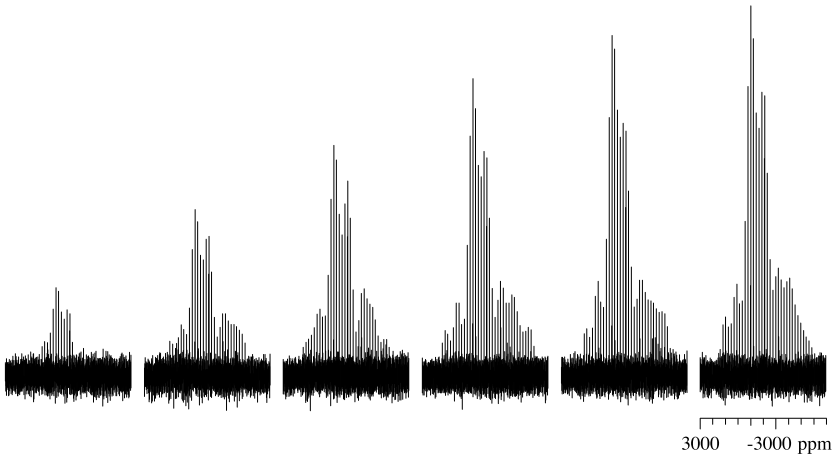

Figure 3. A series of experimental 19.6 T (54.09 MHz) static QCPMG spectra for sample 1 packed in a 3.2 mm rotor observed using six RD D1 = 1, 3, 5, 7, 9, and 11 s following saturation by rapid pulsing before starting each of the six experiments. These spectra serve to illustrate the T_1QCPMG experiments performed for the four samples in this study. Each of the six spectral results from 7168 scans (i.e., a total of 71.7 h or 3.0 days to complete all six spectra) and the spectra are processed using a line broadening (lb) = 100 Hz and a Fourier number (fn) = 128 K. The extraction of the six $T_1(MoS_2)$ values, to be averaged from the exponential fits for the six selected "spikelets", is illustrated in Figure 4.

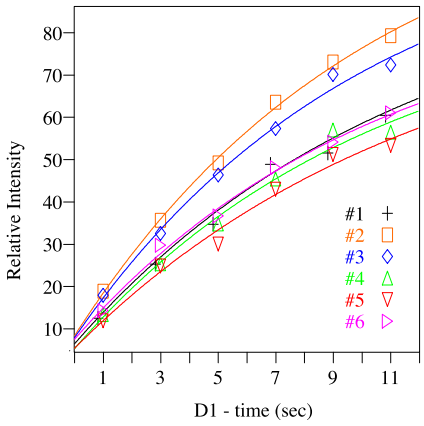

Figure 4. Six $T_1(MoS_2)$ values determined from optimized exponential fits for the consecutive six intense peak heights for the "spikelets" to a high frequency from the rf carrier-frequency (center) of the spectra in Figure 3. The six slightly different $T_1(MoS_2)$ values are 10.3, 10.2, 11.6, 10.6, 10.6, and 12.2 s, giving a mean value $T_1(^{95}Mo)$ = 10.9 ± 1.6 s at 19.6 T for sample 1. The numbering of the six consecutive "spikelets" starts with #1 (in black) being the neighbor "spikelet" to high frequency from one of the largest peak heights (i.e., #2 in orange), followed by the "spikelet" of the second largest height (i.e., #3 in blue). The remaining three consecutive "spikelets" (#4–#6) continue with #6 ending at the position of the rf-carrier frequency.

phonon relaxation constitute the relaxation mechanisms in 2H-MoS_2 materials.

For the present determination of $T_1(^{95}Mo)$ for sample 1 at 19.6 and 35.2 T and otherwise under exact identical conditions (e.g., both at room temperature), the ratio for the two T_1^{CSA} contributions at these magnetic fields is calculated using eq 1 in a straightforward way to be $T_1^{CSA}(19.6\ T)/T_1^{CSA}(35.2\ T) = B_0(35.2\ T)^2/B_0(19.6\ T)^2 = 35.2^2/19.6^2 = 3.23$. This value is slightly lower than the experimentally determined ratio $T_1^{CSA}(19.6\ T)/T_1^{CSA}(35.2\ T) = 10.9/2.8 = 3.89$ (Table 3). However, considering the error limits (±15%), our experimental values actually appear to be in excellent agreement with the predicted theoretical ratio. Thus, we have good reasons to assume that T_1^{CSA} is the main mechanism

Table 3. Summary of the $T_1(^{95}Mo)$ Spin–Lattice Relaxation Times Determined for the Four Different Samples (Samples 1–4) in This Research Using the T_1QCPMG Pulse Sequence at 19.6 T and Also for the Two 2H-MoS_2-Layered Samples (#1 and #4) at 35.2 T[a]

$T_1(^{95}Mo)$ (s)	19.6 T	35.2 T
#1/160-layer	10.9 ± 1.6	2.8 ± 0.4
#2/pseudo-amorph.	2.8 ± 0.4	[b]
#3/Al_2O_3–MoS2 cat.	3.2 ± 0.5	[b]
#4/004-layer	4.5 ± 0.8	1.5 ± 0.2

[a]The $T_1(^{95}Mo)$ values are in seconds (s) including the indicated error limits. The error limits for all samples are all <±15%. [b]The limited time slots allocated for the $T_1(^{95}Mo)$ experiments at 35.2 T and shut down of the SCH magnet during the Covid-19 pandemic did not allow these experiments to be carried out at 35.2 T for sample 2 and sample 3 at this time. However, considering the identical CSA and EFG spectral parameters determined for the four different samples (Table 1) and therefore the identical local Mo electronic environment for these samples, there is good evidence to believe that the $T_1(^{95}Mo)$ relaxation mechanism for sample 2 and sample 3 is also identical to that for sample 1 and sample 4, that is, T_1^{CSA} (see the text).

contributing to the T_1 relaxation for the 160-layer MoS_2 (sample 1) reported here. This exfoliated sample originates from a source for the natural MoS_2 mineral containing a higher-layer 2H-MoS_2 structure, which apparently has been used in earlier studies.[11−13] Holding on to the assumption that T_1 relaxation for high multilayered MoS_2 samples is completely governed by the T_1^{CSA} mechanism, it would be of interest to apply the two T_1 values determined at two different B_0 fields for sample 1 listed in Table 3 for estimation of the $T_1^{CSA}(MoS_2)$ values for sample 1 at the different low B_0 fields used in the earlier studies of high multilayered MoS_2 samples.[10−14] Similarly, for comparison with the estimated/determined T_1 values reported in two of these low-B_0 field studies,[11,13] a calculation/prediction using these two values to obtain the corresponding values at high B_0 fields is of interest. As above, T_1^{CSA} is assumed to be the single relaxation mechanism for all T_1 values in these simple calculations and comparisons employing the proportionality of $1/T_1^{CSA}$ and B_0^2. The calculated and predicted $T_1^{CSA}(MoS_2)$ spin–lattice relaxation

https://doi.org/10.1021/acs.jpcc.0c10522
J. Phys. Chem. C 2021, 125, 7824−7838

times at different B_0 fields are summarized in Table 4 for the two layered samples (sample 1 and sample 4) studied here at

Table 4. Predicted $T_1(^{95}Mo)$ Spin−Lattice Relaxation Times at Different Magnetic Field Strengths (B_0) for the Two 2H-MoS_2 Layer Samples Investigated in This Study (#1 and #4) and for Two High Multilayer 2H-MoS_2 Samples Previously Reported in the Literature[11,13a]

$T_1(^{95}Mo)$ (s)	35.2 T	19.6 T	14.1 T	9.4 T	8.02 T
#1/160-Layer	***2.8***	9.0	18	39	54
#1/160-Layer	3.4	***10.9***	21	47	65
160-Layer (Mean Values)	3.1	10.0	20	43	60
160-Layer (10.0/3.1=3.23)	***3.1***	***10.0***	19	43	60
#4/4-Layer	***1.5***	4.8	9.3	21	29
#4/4-Layer	1.4	***4.5***	8.7	19	27
4-Layer (Mean Values)	1.45	4.65	9.0	20	28
4-Layer (4.65/1.45=3.21)	***1.45***	***4.65***	9.0	20	28
Sample from Bastow[11]	11	37	71	***160***	220
Sample from Tenne[13]	13	43	83	185	***255***

[a]The predicted $T_1(^{95}Mo)$ values for each sample are obtained from a specific $T_1(^{95}Mo)$ value (shown in red) determined at a particular B_0 field and assuming the use of eq 1 (i.e., T_1^{CSA} only), as described in the text. The $T_1(^{95}Mo)$ values are in seconds (s). The value $T_1(^{95}Mo)$ = 160 s at B_0 = 9.4 T is estimated based on the RD of 480 s used for the sample from Bastow,[11] and further with our assumption of a general use of RD ~3 × $T_1(^{95}Mo)$ leading to $T_1(^{95}Mo)$ ~160 s (see also the text).

19.6 and 35.2 T, and for two high multilayered MoS_2 mineral samples previously reporting estimated[11] and measured[13] T_1 spin−lattice relaxation times at 9.4 and 8.02 T, respectively. For each row in Table 4, the number marked in red/italics shows the experimental value measured at the indicated B_0 field and used to calculate the predicted T_1^{CSA} values at the remaining B_0 fields in that particular row. For sample 1 and sample 4, with assumed T_1^{CSA} values measured at two quite different B_0 fields, it appears appropriate to use the mean of the values at the different B_0 fields from these two measurements (although quite similar) as the optimum predicted T_1^{CSA} values at lower B_0 fields. These mean T_1^{CSA} values are listed in the third row for sample 1 and sample 4. It is noted that the mean T_1^{CSA} values at 35.2 and 19.6 T for sample 1 and sample 4 both are well within the error limits for the measured experimental values (Table 3) and that the ratio of these values exactly matches the theoretical value for the ratio between B_0^2 for the two fields, that is $[35.2/19.6]^2$ = 3.23. This follows from the values presented in row 4 of Table 4 for each of the two samples. The predicted T_1^{CSA} values presented in Table 4 for sample 1 and sample 4 give full support for the assumption that the experimental T_1 spin−lattice relaxation times for these samples are dominated by the T_1^{CSA} relaxation mechanism. The results show that the magnitude of T_1^{CSA}, for a particular B_0 field, decreases with decreasing number of layers for the 2H-MoS_2 samples. This statement is supported by the calculated high field T_1^{CSA} values (Table 4) from the low-field T_1 data (9.4[11] and 8.02 T[13]) for multilayered mineral MoS_2 samples; that is, first evidence of a tuning option for an electronic band gap correlation with the number of layers (T_1^{CSA} or B_0) in 2H-MoS_2 samples. For an easier and more comprehensive understanding of the $T_1(^{95}Mo)$ data in Table 4, plots for the $T_1(^{95}Mo)$ relaxation times versus the relative τ_c/τ_c^T correlation times for the four samples at the three selected B_0 fields of 14.1, 19.6, and 35.2 T are displayed in Figure 5. Calculations of

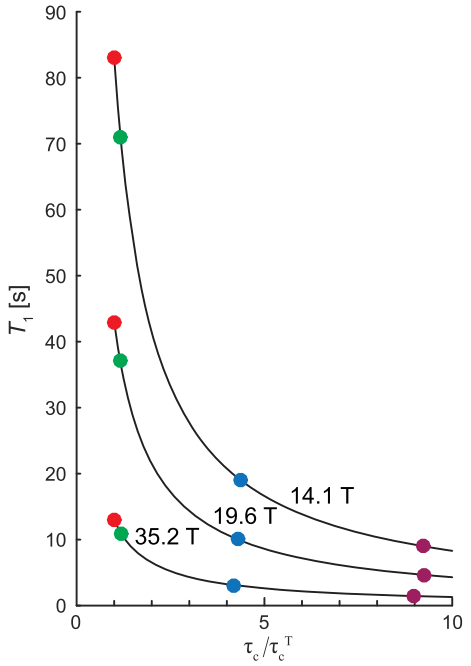

Figure 5. Plots of the $T_1(^{95}Mo)$ spin−lattice relaxation times versus the relative τ_c/τ_c^T correlation times at B_0 magnetic field strengths of 14.1 T, 19.6 T, and 35.2 T for the four 2H-MoS_2 samples (samples 1 and 4; refs 11 and 13) listed in Table 4 (and Table S1) and their $T_1(^{95}Mo)$ data elaborated on in the Supporting Information (pp. S3−S6). The three experimental points (τ_c/τ_c^T, T_1) for each of the four MoS_2 samples are color coded as follows: sample from Tenne:[13] red ●; sample from Bastow:[11] green ●; sample #1, 160-layer: blue ●; sample #4/4-layer: purple ●. Derivations of the expressions for the three B_0 curves are shown in the Supporting Information. For 14.1 T: $T_1 = 83/(\tau_c/\tau_c^T)$, eq S4; 19.6 T: $T_1 = 43/(\tau_c/\tau_c^T)$, eq S5; 35.2 T: $T_1 = 13/(\tau_c/\tau_c^T)$, and eq S6.

the relative correlation time τ_c/τ_c^T and of the equations for the three $T_1(^{95}Mo)$ plots of the four 2H-MoS_2 layered samples using the Table 4 data are outlined in the Supporting Information (see, pp S2−S6). At this point, we just mention that τ_c is referenced to the shortest τ_c determined at all B_0 field strengths (τ_c/τ_c^T), where $\tau_c^T = \tau_c^{Tenne}$ is the value obtained for Tenne and co-worker's sample[13] at a particular B_0 field (Supporting Information, pp S4). The experimental points (τ_c/τ_c^T, T_1) determined for the four 2H-MoS_2 samples at 14.1, 19.6, and 35.2 T (Supporting Information, Table S1) are shown on the three B_0 curves in Figure 5. Most importantly, it is noted that each of the four samples exhibits a particular and identical τ_c/τ_c^T value at the three B_0 field strengths. This shows that the electronic band gap for a particular 2H-MoS_2 sample is not affected by B_0 magnetic field strengths as speculated on in the early stage of this research.

Sample 2: Pseudo-amorphous MoS_2 Nanoparticles and Sample 3: a Surface MoS_2-Layer Catalyst on an Al_2O_3 Support. The solid-state ^{95}Mo NMR results for sample 2 and sample 3 turn out to be quite similar, apart from an obvious difference in NMR sensitivity. From the preliminary 19.6 T ^{95}Mo T_1QCPMG experiments, it was quickly realized

https://doi.org/10.1021/acs.jpcc.0c10522
J. Phys. Chem. C 2021, 125, 7824−7838

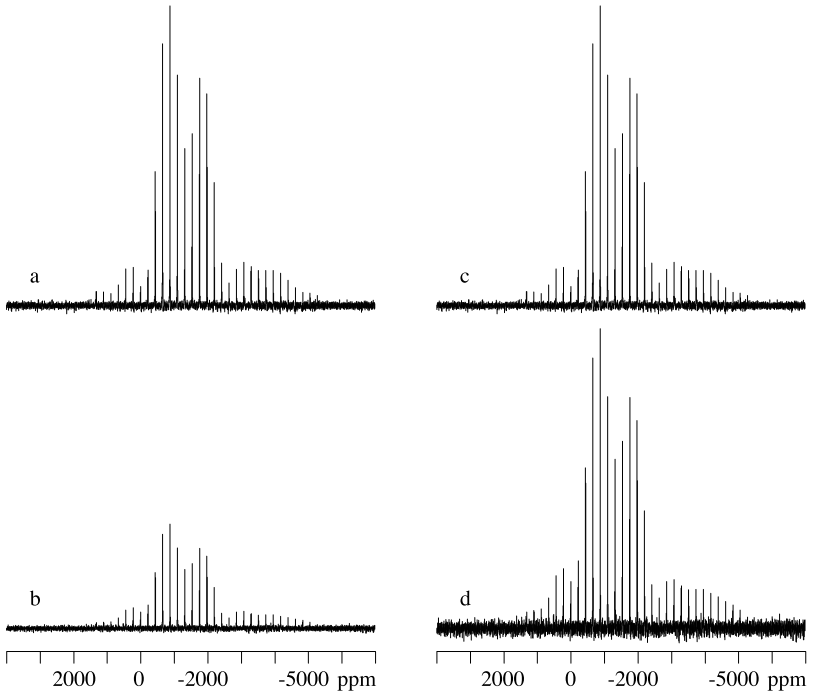

Figure 6. (a) Experimental 19.6 T (54.09 MHz) static QCPMG spectrum for the pseudo-amorphous MoS_2 sample (sample 2) packed in a 3.2 mm rotor, observed using 4096 scans in just 8 h for a RD D1 = 7 s. It is noted that this spectrum represents the last QCPMG spectrum observed in a T_1QCPMG experiment for array D1 = 1, 3, 5, and 7 s, using 4096 scans for each array value in a total of 18.2 h for the complete T_1QCPMG experiment (i.e., an overnight run). (b) Experimental 19.6 T (54.09 MHz) static QCPMG spectrum for the MoS_2−Al_2O_3 catalyst sample (sample 3) packed in a 3.2 rotor, observed using 10,240 scans in 19.9 h for a RD D1 = 7 s. Again, as for (a), this spectrum represents the last QCPMG spectrum observed in the T_1QCPMG experiments for array D1 = 1, 3, 5, and 7 s, using 10,240 scans for each array value, that is, a total of 45.5 h for the complete T_1QCPMG experiment. (c) Copy of the spectrum in (a). (d) Copy of the spectrum in (b) following vertical expansion by a factor of 2.8 (see the text). A line broadening lb = 100 Hz was applied to all spectra in figure.

that an array of only four D1 values (D1 = 1, 3, 5, and 7 s) is required to obtain decent $T_1(^{95}Mo)$ values for both samples. The static ^{95}Mo T_1QPMG spectra corresponding to the array value D1 = 7 s for sample 2 and sample 3 are illustrated in Figure 6 (vide infra) and exhibit a mutual and excellent overall spikelet "fingerprint", which is identical to the D1 = 11 s spectrum in Figure 3 for sample 1 at 19.6 T. As seen from Table 3, $T_1(^{95}Mo)$ ∼3.0 s is obtained for both samples at 19.6 T. Most importantly, it is noted that this low $T_1(^{95}Mo)$ value for these two samples is identical to the value $T_1(^{95}Mo)$ = 2.8 ± 0.4 s determined for the 160-layer MoS_2 sample (sample 1) at 35.2 T. This should make nano-sized MoS_2 materials (e.g., amorphous and surface MoS_2 samples) potentially amenable for solid-state ^{95}Mo NMR studies at today's standard magnetic field strengths (9.4−20 T) as opposed to the higher magnetic field of 35.2 T employed in this research (vide supra). Thus, the T_1QCPMG data for sample 2 and sample 3 (Table 3) are unavailable at 35.2 T (SCH magnet is shut down due to the Covid-19 pandemic).

The D1 = 7 s QCPMG spectra observed at 19.6 T for sample 2 and sample 3 are shown in Figure 6a,b, respectively. These spectra were obtained using exactly identical conditions and acquired immediately succeeding one another, with the only exception being for the number of scans (ns) with ns = 4096 and 10,240 for sample 2 and sample 3, respectively. To obtain the relative MoS_2 concentrations in the two samples, the spectra in Figure 6a,b is plotted in an absolute intensity mode, which reflects the different ns-values for the spectra in their respective noise level (i.e., $[10{,}240/4096]^{0.5}$ = 1.58, a factor of higher noise level in Figure 6a compared to Figure 6b). Thereby, the mole MoS_2 ratio has been obtained directly from the ratio of corresponding peak heights in the two spectra using mean values for the nine most intense peak heights in the center parts of the spectra. This gives a value of the mole MoS_2 ratio for sample 2 (mol)/sample 3 (mol) = 2.8/1. The QCPMG spectra presented in Figure 6c,d serve to illustrate an exact MoS_2 structural identity for sample 2 and sample 3 by the facts that Figure 6c is a copy of the spectrum shown in Figure 6a and that Figure 6d represents the spectrum in Figure 6b after vertical expansion by a scaling factor of 2.8. Thus, with the clear identity observed for these two samples from the QCPMG spectra in Figure 6, the spectra in Figure 6 represent yet another manifestation of the huge sensitivity gain that can be achieved in many areas of ordinary solid-state NMR experiments employing QCPMG techniques.[19−21]

The experimental 19.6 T solid-state ^{95}Mo MAS NMR spectrum for the pseudo-amorphous MoS_2 material (sample 2) is shown in Figure 7a. An optimized simulated spectrum of the experimental spectrum, employing the CT and only the inner STs, is displayed in Figure 7b. The corresponding optimized spectral parameters are listed in Table 1. These values are all within the error limits for the parameters of the MoS_2 160-layer sample (sample 1) determined at 14.1 and 35.2 T. A most noticeable effect observed during the simulation of the experimental spectrum in Figure 7a is a large increase for the line width (i.e., ∼3800 Hz or ∼70 ppm, excluding the artificial line broadening of lb = 1000 Hz employed for the spectra in Figure 7a). This line width of 70 ppm for sample 2 at 19.6 T is more than a factor of 8 higher compared to the estimated line width of ∼8 ppm for sample 1. This increase in line width

https://doi.org/10.1021/acs.jpcc.0c10522
J. Phys. Chem. C 2021, 125, 7824−7838

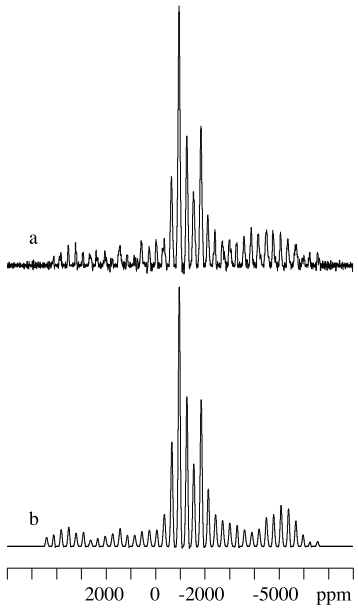

Figure 7. (a) Experimental 19.6 T (54.09 MHz) ^{95}Mo MAS NMR spectrum for the pseudo-amorphous sample of MoS_2 (sample 2). The spectrum was acquired using ns = 78,986 scans in almost 44 h with a RD D1 = 2 s, ν_r = 16.0 kHz, and lb = 1000 Hz. (b) Corresponding simulated spectrum for the CT and inner STs only with optimized fitting of all quadrupole coupling and chemical shift parameters summarized in Table 1 for sample 2. These parameters are all within the error limits of the values reported for sample 1 at 14.1 and 35.2 T in Table 1.

becomes an important issue in the interpretation of the spectra acquired for samples 2−4 at 35.2 T (vide infra). At this stage, we note an obvious effect of this line broadening not only on the disappearance of the outer STs (omitted in the optimized fit), but also on the appearance of the inner STs.

With the above solid-state ^{95}Mo NMR information available on the MoS_2 sample identity for sample 2 and sample 3, obtained from the QCPMG spectra in Figure 6, this serves as an appropriate example of the sensitivity gain achieved by QCPMG compared to the alternative experiment of ^{95}Mo MAS NMR spectroscopy. For this comparison, the experimental 19.6 T ^{95}Mo MAS NMR spectrum of sample 2 shown in Figure 7 (ns = 78,986 and D1 = 2 s, corresponding to an experiment time of 44 h) forms the basis for an estimation of the time required for sample 3 to reach a similar S/N ratio as for sample 2 in Figure 7. Based on the reduced mole MoS_2 content in sample 3 compared to sample 2 by a factor of 2.8, it is estimated that the number of scans required for sample 3 at 19.6 T to achieve this goal must be increased by a factor 2.8^2 = 7.84. Using identical experimental conditions for sample 3 as for sample 2 in Figure 7, this requires ns = 619,250 and thus a corresponding time of the ^{95}Mo MAS experiment for sample 3 of 344 h or about 14 days. Because of the excessively long spectrometer time estimated for a standard ^{95}Mo MAS NMR experiment of this surface MoS_2-layer on a Al_2O_3 support, this experiment was never executed, in particular considering the time of only 28 h required for the acquisition of both static QCPMG spectra in Figure 6a,b. Alternatively, it was decided to test the performance for the somewhat more time-efficient combination of the MAS experiment with QCPMG (known as MAS-QCPMG[19]) for the surface MoS_2−Al_2O_3 sample (sample 3). The reason is that a positive outcome of such an experiment would represent the first example ever for observation of a MAS spectrum at natural-abundance for a low-γ quadrupolar-nucleus species layered on a catalyst support. This first 19.6 T ^{95}Mo MAS-QCPMG NMR spectrum for the very important HDS catalyst, represented by sample 3, is shown in Figure 8b and was acquired by employing

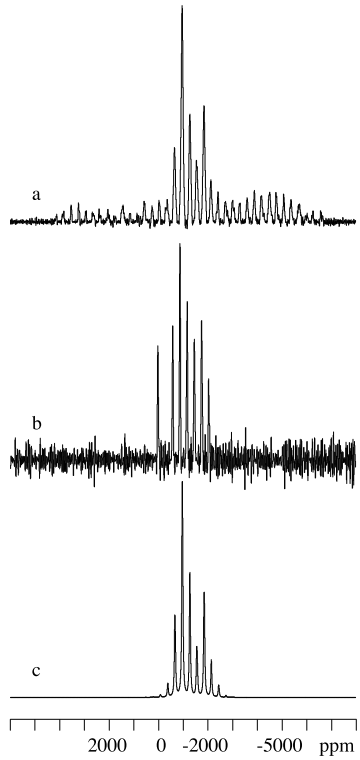

Figure 8. (a) Experimental 19.6 T (54.09 MHz) ^{95}Mo MAS NMR spectrum in Figure 7a for the pseudo-amorphous MoS_2 sample (sample 2) is shown here for comparison with the ^{95}Mo MAS-QCPMG spectrum obtained for the surface MoS_2−Al_2O_3 sample (sample 3) below. (b) Experimental 19.6 T (54.09 MHz) ^{95}Mo MAS-QCPMG NMR spectrum for sample 3 using ν_r = 15.6 kHz, D1 = 3.0 s, and ns = 79,872 (i.e., 2 days and 19 h during a long weekend). An extremely narrow line width of only ∼1000 Hz/∼18 ppm is observed for the ssbs of the line shape for the CT due to the use of MAS-QCPMG as opposed to MAS alone. Also, the narrow resonance at −71 ppm is caused by a minor MoO_4 oxidation product of sample 3 (see the text and Figure 10). (c) Simulation of the central transition (CT) only in the simulated MAS spectrum for sample 2 in Figure 7b and used here to illustrate the obvious "fingerprint" appearance of the "two triplets" for the CT in the spectra of Figure 7a,b at 19.6 T (54.09 MHz).

synchronization of the MAS rotor frequency (ν_r = 15.6 kHz) with the "spikelet" frequency during 2 days and 19 h of data acquisition (see the Figure 8 caption). This impressive spectrum in Figure 8b is accompanied by a copy (Figure 8a) of the ^{95}Mo MAS spectrum for sample 2 shown in Figure 7a and by a simulated spectrum in Figure 8c for the CT only spectrum corresponding to the simulation in Figure 7b. Finally, the experimental MAS-QCPMG spectrum in Figure 8b, as well as the simulation in Figure 8c, exhibits a characteristic line shape of "two tilted triplets", a line shape also observed for the 19.6 T low-intensity ^{95}Mo MAS spectrum for sample 4 in Figure 10b (vide infra). The extremely narrow ^{95}Mo resonance (a line width of ∼12 ppm) observed at −71 ppm, that is, close to the external 2.0 M aqueous Na_2MoO_4 reference, after

https://doi.org/10.1021/acs.jpcc.0c10522
J. Phys. Chem. C 2021, 125, 7824−7838

storage of sample 3 for 2−3 months, is ascribed to a MoO_4^{2-} species, which results from atmospheric air oxidation. This minor MoO_4^{2-} impurity is not observed for sample 2 within 1 month following its synthesis (see Figure 7). However, the same MoO_4 impurity is also clearly observed when recording a 35.2 T ^{95}Mo MAS spectrum of sample 2 about 4 months after its synthesis (see Figure 11, vide infra). However, a very minor impurity has earlier been noted from PXRD and chemical analysis of similarly synthesized MoS_2 HDS catalysts following long-time storage under ambient conditions as in the present studies, the origin and identity of this impurity has remained unknown until it appeared in the present ^{95}Mo NMR study.

Finally, we conclude that the MoS_2 identity of sample 2 and sample 3 may be quickly proven using the ^{95}Mo QCPMG spectra as shown in Figure 6 and further related to the structure for sample 2 through its experimental and simulated ^{95}Mo MAS spectra presented in Figure 7 and the spectral parameters collected in Table 1. It should be mentioned that a structural identification for the two samples may alternatively be obtained directly from MAS-QCPMG experiments as shown in Figure 7 or from simulations of the QCPMG spectrum.[19−21] Such a simulation for the CT in the experimental QCPMG spectrum of Figure 6a for sample 2 is presented in Figure 9 and employs the parameters in Table 1 derived from its ^{95}Mo MAS spectrum and the experimental conditions for the QCPMG experiment (see the Experimental Section).

Sample 4: MoS_2 4-Layer Sample. *Sample 4 and Sample 2 at 19.6 T.* Following the successful acquisition of a 19.6 T ^{95}Mo MAS spectrum for the pseudo-amorphous sample (sample 2) presented in Figure 7, a similar spectrum was expected for the MoS_2 4-layer sample (sample 4) at 19.6 T. While quite an equal number of MoS_2 moles are contained in the fully packed 3.2 mm rotors for the two samples (samples 2 and 4), and both have a similar low T_1 value (3−5 s, see Table 3), it was a surprise to observe the reduced intensity in the 19.6 T ^{95}Mo MAS spectrum for sample 4 (Figure 10b). Assuming about equal weights for the two samples have been packed into the two 3.2 mm rotors, the spectra in Figure 10a,b are plotted on an absolute intensity scale, which reflects the difference in MoS_2 signal intensities for the two samples and the slightly increased noise level by a factor $[78{,}986/45{,}994]^{0.5} = 1.31$ for the spectrum in (b) compared to (a). Thus, the intensity ratio determined from the resonance signals for the CTs (again with the line shape for the "two tilted triplets" as observed for all the spectra in Figure 8) in the spectrum of Figure 10a,b, we found that the ^{95}Mo MAS NMR intensity for Sample 4 is reduced by a factor of ∼2.35 compared to that for sample 2. Most importantly, we note that the line width (excl. the artificial lb = 1000 Hz) observed for the "fingerprint" of the "two triplet" line shape constituting the CT for sample 4 is ∼3800 Hz (i.e. ∼70 ppm) similar to that observed for sample 2. Simultaneously, we found that the special band-shape pattern created by the spinning sidebands (ssbs) for the inner STs continues the tendency of blurring in going from sample 2 to sample 4 as observed in Figure 11a,b and from comparison with a spectral simulation, which includes the STs (e.g., in Figure 8b). In the spectrum for sample 4 (Figure 11b), the intensities for the inner STs have become so indistinct (or are even obscured into the noise) that they cannot be used in an optimized fit to obtain reliable spectral parameters. Thus, for sample 4, we rely on the "fingerprint" of "two tilted triplets" observed for the CT

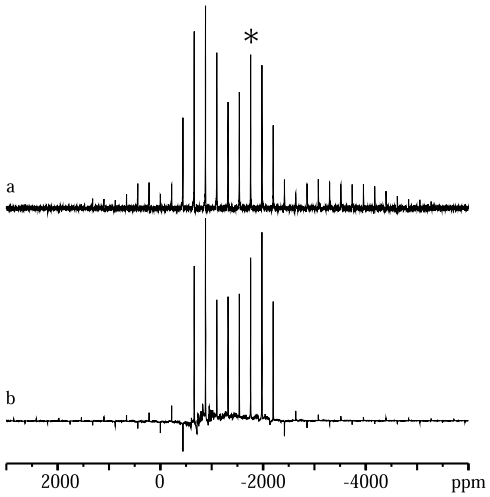

Figure 9. Comparison of the experimental (a) and simulated (b) 19.6 T (54.09 MHz) static ^{95}Mo QCPMG NMR spectrum for the experimental QCPMG spectrum of sample 2 presented in Figure 6a. (b) Simulated QCPMG spectrum is calculated for the CT only, as used elsewhere,[19−21] and employed the spectral parameters in Table 3 for sample 2, along with the following experimental rf parameters related to the QCPMG pulse sequence: transmitter offset (*) at −1758 ppm, dwell time = 1 μs (spectral width = 1.0 MHz), number of echoes = 200, number of points in each echo envelope = 84, P1 = P2 = P3 = 4 μs, $\gamma B_1/2\pi$ = 25 kHz, and a Gaussian lb = 125 Hz. These parameters are all very similar to the actually used experimental parameters (see the Experimental Section). The differences between the experimental and simulated "spikelet" intensities are due to the fact that the experimental spectrum represents an overlap of the CT and ST "spikelet" spectra, while our simulation software was developed to include the CT-only and for quite large C_Q values.[19−21]

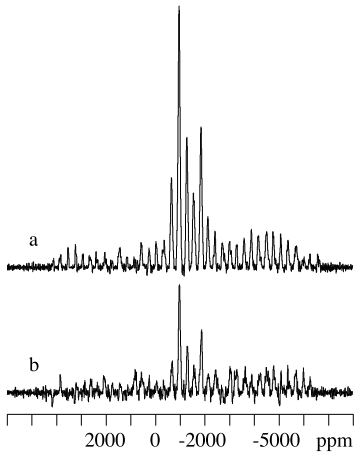

Figure 10. (a) Copy of the experimental 19.6 T (54.09 MHz) ^{95}Mo MAS NMR spectrum shown in Figure 7a of the pseudo-amorphous MoS_2 sample (sample 2), ns = 78,986, for comparison with the corresponding experimental spectrum shown here in (b) for the 4-layer MoS_2 sample (sample 4). (b) Experimental 19.6 T (54.09 MHz) ^{95}Mo MAS NMR spectrum for the 4-layer MoS_2 sample (sample 4) acquired for ns = 45,994 in about 26 h with a RD D1 = 2 s, ν_r = 16.0 kHz, lb = 1000 Hz, and using the same rf pulse conditions as for sample 2 in (a). The spectra in (a,b) are plotted in an absolute intensity mode, which reflects the influence of the different ns values on the noise levels in their respective spectra and therefore the observed relative MoS_2 intensities from ^{95}Mo MAS NMR of the two samples (see the text).

https://doi.org/10.1021/acs.jpcc.0c10522
J. Phys. Chem. C 2021, 125, 7824−7838

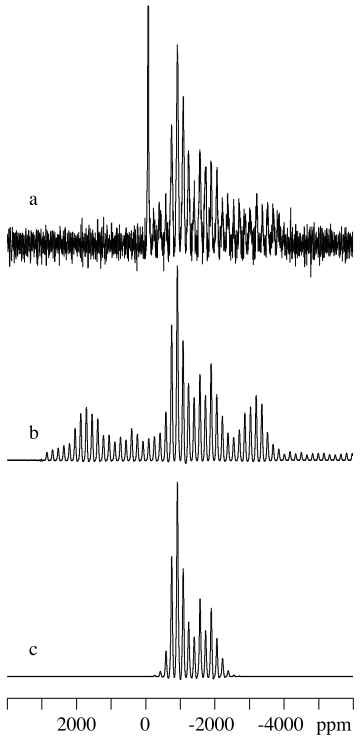

Figure 11. (a) Experimental 35.2 T (97.63 MHz) ^{95}Mo MAS NMR spectrum for the pseudo-amorphous sample of MoS_2 (sample 2). The spectrum was acquired using 4096 scans in 2.3 h with a RD D1 = 2 s, ν_r = 16.0 kHz, and lb = 500 Hz. The extremely narrow resonance at −71 ppm [(a line width of ∼1200 Hz/12 ppm excluding the artificial line broadening caused by a minor MoO_4 oxidation product of sample 2 (see the text)] has been cut off at 50% of its height. In contrast, the line width for the main CT resonances at −1000 ppm for sample 2 is ∼5600 Hz/57 ppm. (b) Simulated 35.2 T (97.63 MHz) ^{95}Mo MAS NMR spectrum for the central (CT) and inner satellite (ST) transitions for sample 2, employing the spectral parameters for the same sample 2 determined here at 19.6 T (Table 1; see Figure 5b) converted to the 35.2 T simulation presented here in Figure 11b. (c) Simulation of the corresponding simulation in (b), but only for the CT at 35.2 T (97.63 MHz).

and the corresponding simulated CT spectrum shown in Figure 8c employing the spectral parameters determined for sample 2 (Table 1).

At this stage, it seems appropriate to partly summarize the most important trends observed in the results of the solid-state ^{95}Mo NMR studies for samples 1−4, before advancing to a study of sample 2 and sample 4 at 35.2 T. In the ^{95}Mo MAS NMR spectrum of sample 1 at 35.2 T, a moderate increase in the line width for the ssbs to ∼1450 Hz (∼15 ppm) compared to the line width of ∼250 Hz (∼6 ppm) observed for sample 1 at 14.1 T,[11] that is, an increase by a factor of 2.5, which matches the ratio between the two magnetic field strengths. For these narrow line widths, the optimized fitting of the experimental spectra for sample 1 at 14.1 and 35.2 T both employed the CT and all the inner and outer STs, as for example is clearly observed from the spectra presented in Figure 2 of this research. For sample 2 and sample 4, a much larger line width is observed at 19.6 T and with identical line widths of ∼3800 Hz (∼70 ppm) for the resonance lines within the "two tilted triplets" of the CTs. While the large increased line broadening is not much of a surprise for the CT in both of the two samples, the observed decreased MoS_2 intensity by a factor of ∼2.35 for the CT in sample 4, compared to sample 2, was initially more of a surprise. In addition, while the ^{95}Mo MAS NMR spectrum for sample 2 served useful for an optimized fit of the spectral parameters, employing both the CT and inner STs (vide supra, Figure 8), this was not possible for the corresponding ^{95}Mo MAS NMR spectrum of sample 4, because of the increased blurring of the ssb intensities for the inner STs in this sample (vide supra, Figure 11). However, our expectations were still fairly high at the onset of the investigation for the spectral behavior and results for sample 2 and sample 4 at 35.2 T.

Sample 4 and Sample 2 at 35.2 T. With the higher quality obtained for the ^{95}Mo MAS NMR spectrum for sample 2 at 19.6 T of the two samples, it seemed obvious to start out with a study of sample 2 at 35.2 T. Thus, the 35.2 T ^{95}Mo MAS NMR spectrum (ν_r = 16.0 kHz) of the pseudo-amorphous sample (sample 2) observed after 2.5 h of spectrometer time is presented in Figure 12a (details of the acquisition and

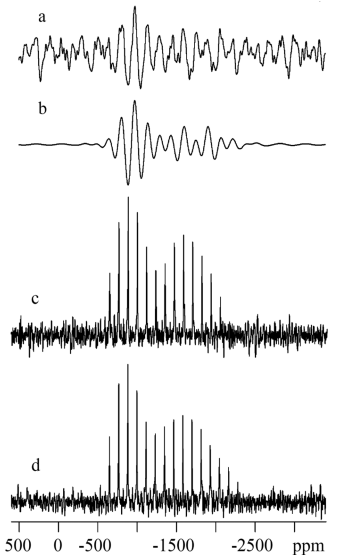

Figure 12. Experimental 35.2 T (97.63 MHz) ^{95}Mo MAS and static QCPMG NMR spectra for the 4-layer MoS_2 sample (sample 4). (a) MAS spectrum (ν_r = 16 kHz) acquired in 2.3 h similarly to sample 2 in Figure 10 but with lb = 1000 Hz and a trapezoidal weight function and an optimized broadening of 7000 Hz to the FID (see the text). (b) Simulation of the MAS spectrum in (a) using the parameters for sample 4 in Table 1, the same trapezoidal weight function and optimized broadening to the FID as in (a). In (c,d), the QCPMG NMR spectra are shown for sample 4 (c) and the 160-layer MoS_2 sample 1 (d) each packed in a 3.2 mm rotor, each using 256 scans, D1 = 7 s, lb = 500 Hz; i.e., only 30 min for each spectrum. We note that (c,d) QCPMG spectra shown here represent the last D1 = 7 s value used in the D1-array (1, 3, 5, and 7 s) for the T_1QCPMG experiments at 35.2 T with 256 scans for each array value. These values result in a total of 68 min to complete each T_1QCPMG experiment (see Table 4 for the T_1(^{95}Mo) spin−lattice relaxation times determined at 35.2 T for the two samples from these experiments).

processing parameters are given in the figure caption). At this point in time, the data acquisition was stopped because it became obvious that a spectrum of sufficient and the expected higher quality at 35.2 T, compared to that for sample 2 at 19.6 T (Figure 7) for extraction of the spectral parameters, could not be achieved in an acceptable time. On the other hand, the present experimental spectrum (Figure 10a) along with the simulated spectrum in Figure 10b provide some important

https://doi.org/10.1021/acs.jpcc.0c10522
J. Phys. Chem. C 2021, 125, 7824−7838

information, which could have serious impacts on the possibilities for even observing a ^{95}Mo MAS NMR spectrum for sample 4 at 35.2 T. The simulated ^{95}Mo MAS NMR spectra in Figure 11b,c show that a main part of the ssbs for the inner STs in the experimental spectrum (Figure 11a), at least to high frequency from the CT, is heavily blurred/scrambled into the noise level of the baseline. Again, we should point out that the simulation for the CT in Figure 11c clearly recognizes the CT in the experimental spectrum as a "fingerprint" with a width for the CT line shape ranging from −500 to −2300 ppm. Moreover, for sample 2, the additional line broadening of ∼1800 Hz observed for the experimental spectrum at 35.2 T relative to the line width at 19.6 T (Figure 7), that is, (5600−3800) Hz = ∼1800 Hz (∼18 ppm), puts an upper limit of ∼18 ppm for the total dispersion, $\Delta(^{95}\mathrm{Mo})$, in ^{95}Mo chemical shifts, which undoubtedly contribute to the line broadening for sample 2. Such $\Delta(^{95}\mathrm{Mo})$ contributions may arise from ^{95}Mo chemical shift differences for Mo sites positioned at the edges and corners of the nanoparticles and which accordingly may contribute differently to the line broadening dependent on the nanostructures for the individual MoS_2 sample. Finally, we note the appearance of the very narrow MoO_4 resonance at −71 ppm in the ^{95}Mo MAS spectrum for sample 2, approximately 3 months after the first recording of its ^{95}Mo MAS spectrum at 19.6 T in Figure 6, where it is not detected. However, the same narrow resonance was earlier observed for the MoS_2−Al_2O_3 surface sample (sample 3) in Figure 8b, about 3 months following its synthesis.

With the somewhat surprisingly poor quality observed for the ^{95}Mo MAS NMR spectrum of sample 2 at 35.2 T (Figure 11) compared to that at 19.6 T (Figure 7), a dramatic decrease in signal intensity observed for the 35.2 T MAS of sample 4, directly following the acquisition of sample 2, was not quite unexpected based on the reduced intensity (a factor of 2.38) for sample 4 compared to sample 2 at 19.6 T (Figure 10). Following 2.3 h of data acquisition at 35.2 T for sample 4, that is, identical to that for sample 2 at 35.2 T (Figure 11), only an extremely low intensity and a broad line shape is observed in the region from ∼−500 to ∼−2300 ppm. In addition, it was very difficult to arrive at a correct phase correction for the spectrum because of the fact that the free induction decay (FID) displays only a single (i.e., the first and weak) MAS rotational echo after 63 μs, corresponding to ν_r = 16.0 kHz for the applied MAS frequency. The first 10−25 μs of this period is the standard receiver dead time period caused by ring-down of the NMR probe and resulting in serious distortions of the spectrum. As a remedy to partly overcome these distortions, we applied a trapezoidal weight function zeroing the data points for the first 30 μs in the FID for the experimental MAS spectrum. For comparison, we applied this weight function to the FID for the experimental as well as the simulated spectrum. The resulting experimental and simulated spectra, both with a minor "dip" in the baseline around the most intense resonances, are shown in Figure 12a,b, respectively. It is gratifying to note that a comparison of the spectra in Figure 12a,b clearly shows that the experimental 35.2 T ^{95}Mo MAS spectrum for sample 4 represents the predicted spectrum for the CT region only, however, with a tremendous loss in sensitivity (S/N ∼2:1), based on the full width for the line-shape pattern, line widths of the individual ssbs, and finally the separation of 16 kHz for the ssbs for the spectrum in Figure 12a. With reference to the comparison of the 19.6 T ^{95}Mo MAS NMR spectra for samples 2 and 4 in Figure 10, the strikingly lower MoS_2 intensity by a factor of ∼2.35 for sample 4, along with the blurring of the inner STs (Figure 10b) and with a STEM image looking like "crumpled, rose-like, pieces of paper" for this 4-layer sample (Supporting Information, Figure S3), indicate that the number of MoS_2 edge/corner sites is higher in sample 4. In addition, we note that a magnetic field of 19.6 T is not strong enough to induce a significant difference in the line width for the CT resonance (the "two tilted triplets") in both samples because these are ∼3800 Hz for sample 2 and sample 4 at 19.6 T (vide supra). However, at 35.2 T, the line width observed for sample 4 from Figure 12a is ∼7400 Hz, while for sample 2, the line width is ∼5600 Hz at 35.2 T as measured from the spectra in Figure 10. Thus, at 35.2 T, the ^{95}Mo chemical shift dispersion $\Delta(^{95}\mathrm{Mo})$ is larger for sample 4 ($\Delta(^{95}\mathrm{Mo})$ < ∼7600 Hz) compared to the value for sample 2 ($\Delta(^{95}\mathrm{Mo})$ < ∼5800 Hz) by approximately 2000 Hz or 20 ppm. Thereby, the increased number of MoS_2 edge/corner sites (causing the increase in Δ^{95}Mo) for sample 4, as compared to sample 2, accounts for the almost complete disappearance of its ^{95}Mo MAS NMR spectrum at 35.2 T due to blurring or scrambling of the ssbs for all STs and broadening of the CT under the conditions of MAS. Actually, it is believed that it is only a lucky accident that our sample 4 allowed unravelling the extremely weak resonance from the ^{95}Mo MAS spectrum of Figure 12a because it could have been a complete failure (or even more of a success). The proposed correlation between ^{95}Mo MAS line widths and dispersions $\Delta(^{95}\mathrm{Mo})$ in ^{95}Mo isotropic chemical shifts (δ_{iso}) caused by small variations in δ_{iso} for the MoS_2 edge/corner sites as an explanation for the degraded quality of ^{95}Mo MAS NMR spectra of MoS_2 nanomaterials, for example, the sample 4 (4-layer sample), is fully supported by the results obtained for sample 1 (160-layer sample) in this study. First, at 35.2 T, the line width for the 160-layer sample of ∼1450 Hz undergoes an increase for the 4-layer sample to ∼7600 Hz, in agreement with a larger number of MoS_2 edge/corner sites expected solely based on geometry arguments from the ratio 160/4 = 40 for the increased number of edge/corner sites. Second, a ^{95}Mo chemical shift dispersion $\Delta(^{95}\mathrm{Mo})$ = (7600−1450) Hz = 6150 Hz (63 ppm) for sample 4 at 35.2 T relative to the line width of 1450 Hz for sample 1 gives an estimated small $\Delta(^{95}\mathrm{Mo})$ = 63 ppm relative to the width of ∼1800 ppm at 35.2 T for the broad ^{95}Mo static NMR spectrum for sample 1 (Figure 12d). This only ∼3.5% $\Delta(^{95}\mathrm{Mo})$ perturbation for the broad static spectrum for sample 1 indicates that almost identical static spectra would be expected for sample 1 and sample 4 at 35.2 T, as opposed to the dramatic difference demonstrated here for the corresponding two ^{95}Mo MAS spectra acquired here at 35.2 T. Fortunately, a set of static ^{95}Mo NMR spectra for sample 1 (160-layer sample) and sample 4 (4-layer sample) has already been obtained in connection with the static T_1QCPMG measurements for these two samples, which exhibit identical EFG and CSA spectral parameters (Table 1). Assuming approximately equal quantities of sample 1 and sample 4 are packed into their respective 3.2 mm rotors, the static T_1QCPMG ^{95}Mo NMR spectra obtained for D1 = 7 s and using identical experimental conditions are shown in Figure 12c (sample 4) and Figure 12d (sample 1). As expected, the two spectra should show up with an identical appearance (identical "fingerprints"), that is, an identical width of ∼1800 ppm and a band shape for the CTs in the two samples, and last but not least, with a very similar signal-to-noise ratio for the identical experimental conditions used and described in Figure

https://doi.org/10.1021/acs.jpcc.0c10522
J. Phys. Chem. C 2021, 125, 7824−7838

12. As shown in Figure 12, the two QCPMG ^{95}Mo NMR spectra in Figure 12c,d show a clear identity of the molecular compositions for sample 4 and sample 1, respectively. The above discussion illustrates the reason for the somewhat unexpected huge difference observed in the appearance for a static and MAS ^{95}Mo NMR spectrum of a 160- and 4-layer MoS_2 sample (sample 1 and sample 4, respectively) acquired at 35.2 T.

Finally, we point out that the above discussions on the experimental solid-state NMR and high-resolution TEM (HR-TEM)/STEM results (Supporting Information) for our 4-layer 2H-MoS_2 (sample 4) throw further light on an early *Science* report[23] of a poorly crystalline MoS_2 "rag" structure from EM and PXRD methods. We note the identity of the PXRD diagram for sample 2 ("pseudo"-amorphous) and sample 4 (4-layer 2H-MoS_2) shown in the Supporting Information (page S13, Figure S7) is similar to the PXRD diagram for a particular MoS_2 "rag" presented in Figure 4 of this report.[23] Moreover, the "rose-like" or "crumpled" STEM image for sample 4 (Supporting Information, page S8, Figure S3, bottom right) appears similar to the EM images of "folded" few-layered MoS_2 "rag" structures presented in Figures 1−3 by Chianelli et al.[23] Thus, future structural characterization of such "rag" structures may take advantage of the new solid-state ^{95}Mo NMR results achieved in the present research. In particular, the introduction of the ^{95}Mo CSA-phonon T_1-relaxation mechanism for 2H-MoS_2 samples could be useful in determining the stack number of layers for a variety of different layers in MoS_2 "rag" structures, which apparently can be prepared by variation of the heating time and temperature during synthesis.[23]

EXPERIMENTAL SECTION

Materials and Synthesis. Four MoS_2 samples were prepared and characterized using various methods for the present solid-state ^{95}Mo NMR study. Sample 1 is obtained by exfoliation of a MoS_2 US-Arizona mineral sample in super-critical CO_2 and exhibits a layer structure of 160 ± 45 MoS_2 layers as observed by STEM along with a statistical analysis to the edges of the crystallites (see Supporting Information). We note that this is the same sample as used in the 14.1 T study.[14] Sample 4 is a few-layer MoS_2-structure, synthesized in our group at Aarhus University, and has only 4 ± 1.2 MoS_2 layers according to a HR-TEM analysis. A STEM image (see Supporting Information) show these 4-layers look like crumpled pieces of paper with a rose-like look. Details of this synthesis are reserved due to a patent application being prepared. Sample 3, synthesized at Haldor Topsøe (HT) A/S, is MoS_2 supported on a high surface area γ-Al_2O_3 (Brunauer−Emmett−Teller surface area of 280 m^2/g) and is, apart from the absence of paramagnetic Co or Ni promoters, identical to the industrial HDS catalyst produced by HT. It was synthesized by incipient wetness impregnation of γ-Al_2O_3 extrudates using a solution of $(NH_4)_6Mo_7O_{24}{\cdot}4H_2O$ in aqueous ammonium hydroxide ([Mo] = 2.5 mol/L; $[N]_{total}$ = 6.25 mol/L), followed by calcination at 450 °C for 2 h, and after cooling crushed into a fine powder of MoO_3/Al_2O_3. Finally, the MoO_3/Al_2O_3 powder is sulfided for 3 h in a tube furnace at 400 °C by exposure to a gas-stream of 10 mol % H_2S in H_2 followed by passivation at room temperature in a gas-stream of 2 mol % O_2 in N_2 for 2 h before removal of the deep-black MoS_2/Al_2O_3 sample from the tube furnace. Chemical analysis for the MoS_2/Al_2O_3 sample (sample 3) gives a wt % Mo = 14.9% and a wt % S = 10.1%, which correspond to an atomic ratio S/Mo = 2.03, precisely as expected for MoS_2 in the sample. TEM analysis shows the presence of highly dispersed MoS_2 nanoparticles 1−4 layers tall and 1−5 nm wide, in agreement with earlier chemical analysis of ∼2−4 MoS_2-layers on a Al_2O_3-surface support for the HDS catalyst produced by HT. Sample 2 is an additional sample of nano-sized MoS_2 crystals similar to those on the surface MoS_2/Al_2O_3 catalyst of sample 3, however, without a support. The synthesis of this sample employed the same tube furnace sulfidation conditions as carried out above for sample 3 and along with this sample. Thus, a vessel with a batch of solid $(NH_4)_2MoS_4$ was placed in the tube furnace to undergo sulfidation in H_2S/H_2 at 400 °C for 3 h. PXRD of this unsupported MoS_2 sample shows four excessively broadened lines (Supporting Information, page S12, Figure S7) and a 100% pure MoS_2 sample of nano-sized crystallites as expected from this reaction. Thus, we also dub sample 2, the "pseudo-amorphous" sample. TEM analysis of sample 2 shows MoS_2 in the form of 3−5 layer structures that are typically 5−10 nm wide.

Solid-State ^{95}Mo NMR Spectroscopy. The solid-state ^{95}Mo NMR experiments employed in the present study involve both MAS and static QCPMG (quadrupolar Carr−Purcell−Meiboom−Gill) experiments all performed at the NHMFL. Research on the QCPMG technique as a tool for sensitivity enhancement of quadrupolar nuclei was initiated in the late 1990s.[19−21] This method has proven invaluable in the present research, in particular for $T_1(^{95}Mo)$ measurements employing the T_1 saturation-recovery technique. All four MoS_2 samples described in the above section were studied at both 19.6 and 35.2 T, where the studies at 19.6 T were required for the three new samples 2−4 to justify the requirements for spectrometer time at 35.2 T. Sample 1 already passed the requirements.[14] The details of the ^{95}Mo MAS NMR spectroscopy, performed on a Varian Direct-Drive VNMRS-600 spectrometer at 14.1 T for sample 1 (Figure 1), are given elsewhere.[14] The solid-state ^{95}Mo NMR spectroscopy performed for all samples at 19.6 and 35.2 T are outlined separately below for the two corresponding spectrometers. All T_1QCPMG experiments used static samples and were conducted at ambient temperature at 19.6 and 35.2 T.

NHMFL Narrow-Bore 19.6 T Magnet with a Bruker AVANCE NEO Console. Solid-state ^{95}Mo NMR spectra (MAS and QCPMG) on this 19.6 T spectrometer were acquired at 54.090 MHz and at ambient temperature. This spectrometer is equipped with a special Magnex narrow-bore (31 mm i.d.) magnet and a NHMFL designed and built narrow-bore (31 mm o.d.) double-resonance X-{^{1}H} broad-band MAS probe for 3.2 mm o.d. rotors with a sample volume of 30 μL. For MAS NMR, the samples were spun at $\nu_r \sim 16$ kHz using a 3.2 mm o.d. MAS rotor/stator module from Revolution NMR, and employed standard single-pulse excitation. ^{95}Mo chemical shifts (δ_{iso}) were referenced relative to 2.0 M aqueous Na_2MoO_4. However, the actual ^{95}Mo experiments used the ^{17}O NMR resonance of aqueous D_2O as a secondary reference using the ^{95}Mo/^{17}O spectrometer frequency (SF) interconversion: $SF(^{95}Mo) = SF(17O) \times 6.516926/13.556457$.[24] A 90° flip-angle $pw(90)_{liquid}$ = 12.0 μs was obtained at 54.09 MHz ($\gamma B_1/2\pi$ = 21 kHz), while a value of pw = 2.0 μs, corresponding to a liquid 15° flip-angle (or a solids 45° flip angle), was used for the actual ^{95}Mo MAS experiments along with RDs in the range of 1−4 s for the different samples. The number of scans used for the MAS experiments are in the range 8192−73,728 and the actual

https://doi.org/10.1021/acs.jpcc.0c10522
J. Phys. Chem. C 2021, 125, 7824−7838

number for the spectra shown in the text are given in the corresponding figure captions. For the QCPMG pulse sequence at 19.6 T, the three pulses P1, P2, and P3 all have the same length P1 = P2 = P3 = 4 μs, which corresponds to a solid 90° flip angle. The number of points between the pulses P2 and P3 is 84 points using a dwell time of 1 μs (a spectral width of 1.0 MHz). For the $T_1(^{95}\text{Mo})$ spin−lattice relaxation time measurements, employing the QCPMG pulse sequence (T_1QCPMG), generally five different spectra were acquired. These correspond to an increase in the RD of D1 = 1, 3, 5, 7, and 9 s between the QCPMG cycles and thereby the intensity points on the T_1-curve. It is important to note that based on the large low-field (~9.4 T) $T_1(^{95}\text{Mo})$ values for MoS_2[11,13] and without knowledge of the values at much higher fields, the purpose of the present $T_1(^{95}\text{Mo})$, T_1QCPMG experiments is simply to obtain useful $T_1(^{95}\text{Mo})$ values to establish a proper experimental setup for the acquisition of the solid-state ^{95}Mo NMR spectra for the four samples. Thereby, an efficient utilization of the spectrometer time allocated on the two high field spectrometers was achieved. For the same reasons, the array of D1 values shown above was used for all four MoS2 samples at both 19.6 and 35.2 T, with the exception for sample 1 at 19.6 T where the array D1 = 1, 3, 5, 7, 9, and 11 s was used (see Figures 3 and 4).

NHMFL SCH Magnet at 35.2 T with a Bruker AVANCE NEO Console. The solid-state ^{95}Mo NMR spectra (MAS and QCPMG) on this 35.2 T spectrometer were acquired at 97.632 MHz and also, as for the 19.6 T experiments, at ambient temperature. Details of the NHMFL design, construction, and operation of this 35.2 T spectrometer along with its single-resonance 3.2 mm MAS probe, including an external ^{7}Li lock system, are described elsewhere.[18] The high-density MoS_2 (~3.0 g/mL) samples, packed into 3.2 mm o.d. zirconia rotors with a 30 μL sample volume, were spun at MAS frequencies in the range ν_r = 14−16 kHz. Adjustment of the magic-angle setting was performed from the top of the magnet by ^{23}Na MAS NMR for a sample of Na_2SO_4, and for the safety of the operator (in the case of a magnet quench) at a lower magnetic field strength of about 18 T. ^{95}Mo chemical shifts (δ_{iso}) were referenced relative to 2.0 M aqueous Na_2MoO_4. However, the actual ^{95}Mo experiments used the ^{17}O NMR resonance of aqueous D_2O as a secondary reference using the $^{95}\text{Mo}/^{17}\text{O}$ SF interconversion: $SF(^{95}\text{Mo}) = SF(^{17}\text{O}) \times 6.516926/13.556457$.[24] A 90° flip-angle $pw(90)_{liquid}$ = 13.9 μs was determined at 97.632 MHz and corresponds to $\gamma B_1/2\pi$ = 18 kHz. However, a value of pw = 2.0 μs, corresponding to a liquid 13° flip-angle (or a solid 39° flip angle), was used for the actual ^{95}Mo MAS experiments along with RD in the range 1−4 s for the different samples, that is, quite similar conditions as used at 19.6 T. Also, the rf conditions for the QCPMG experiments are very similar to those at 19.6 T, the only exception is that at 35.2 T, the pulse lengths for the three pulses P1, P2, and P3 have been changed to P1 = 4 μs and P2 = P3 = 8 μs and that at 35.2 T, the number of points between the pulses P2 and P3 is 88 points for a dwell time of 1 μs (a spectral width of 1.0 MHz).

Analysis of Solid-State ^{95}Mo NMR Spectra. The analysis of the ^{95}Mo MAS NMR spectra was performed using the STARS software package.[25] The present version of STARS used here has been upgraded during the past few years and is capable of simultaneously handling spectral parameters [i.e., quadrupole coupling (C_Q and η_Q), chemical shift (δ_{iso}, δ_σ, and η_σ), and Euler angles (ψ, χ, and ξ) relating the relative orientation for these two tensorial interactions] for up to eight different nuclear sites in the optimization of a fit to an experimental spectrum. In addition to the spectral parameters, the iterative fitting procedure can also include deviation ($\Delta\theta$) from the magic angle, rf bandwidth, rf offset, jitter in spinning frequency,[26] and the line widths (Lorentzian and/or Gaussian). This upgraded version of STARS has been incorporated into both Varian VnmrJ software running on SUN Microsystems Ultra-5 workstations and VnmrJ software running on a Linux RedHat PC. The quadrupole coupling and CSA parameters are defined by

$$C_Q = eQV_{zz}/h \quad \eta_Q = (V_{yy} - V_{xx})/V_{zz} \tag{2}$$

$$\delta_\sigma = \delta_{iso} - \delta_{zz} \quad \eta_\sigma = (\delta_{xx} - \delta_{yy})/\delta_\sigma \tag{3}$$

$$\delta_{iso} = (1/3)\text{Tr}(\delta) = (1/3)(\delta_{xx} + \delta_{yy} + \delta_{zz}) \tag{4}$$

where $\delta = \lambda$ is the diagonalized CSA tensor when using the general convention for the principal elements ($\lambda_{\alpha\alpha} = V_{\alpha\alpha}$, $\delta_{\alpha\alpha}$) of the two diagonalized interaction tensors (EFG and CSA) in eq 5

$$\begin{aligned} &|\lambda_{zz} - (1/3)\text{Tr}(\lambda)| \\ &\geq |\lambda_{xx} - (1/3)\text{Tr}(\lambda)| \\ &\geq |\lambda_{yy} - (1/3)\text{Tr}(\lambda)| \end{aligned} \tag{5}$$

The relative orientation of the two tensors is described by the three Euler angles (ψ, χ, and ξ), which correspond to positive rotations of the CSA principal axis system around $z(\psi)$, the new $y(\chi)$, and the final $z(\xi)$ axis.

Determination of the $T_1(^{95}\text{Mo})$ spin−lattice relaxation time values from the saturation-recovery T_1QCPMG measurements, followed individually exponential fitting of the peak heights $I(t)$ for 5−6 high-intensity "spikelets", close to the rf carrier-frequency, at the center of the spectrum for each of the D1-values used to characterize the T_1-curve. The fit of the peak heights $I(t)$ for a single "spikelet" as a function of t (i.e., the D1-values) followed a three-parameter optimization to the exponential function $I(t) = (A_1 - A_2)\exp(-t/T_1) + A_2$ for the variables A_1, A_2, and T_1. Here, $A_1 = 0$ for $t = 0$ corresponds to $I(0) = 0$ (i.e., complete saturation at $t = 0$), A_2 corresponds to t = infinitive (i.e., completely relaxed magnetization), and the optimized $T_1 = T_1(^{95}\text{Mo})$. The $T_1(^{95}\text{Mo})$ values, reported here in Table 3 for each of the four investigated samples, represent a mean value of the 5−6 different "spikelet" values determined for each sample including the averaged error value.

CONCLUSIONS

For the first time since the pioneering solid-state ^{95}Mo NMR studies on multilayered MoS_2 samples performed during the 1990−2010 decades by independent research groups[10−14] to determine the EFG and CSA for such samples, the present research on four different MoS_2 nanomaterials represents a breakthrough in characterizing fundamental MoS_2 nanostructures according to their different ^{95}Mo NMR characteristics influenced by (i) their method of synthesis, (ii) their different structures, and (iii) the applied magnetic field. Employing the standard pulse sequences of MAS, QCPMG, and MAS-QCPMG to solid-state ^{95}Mo NMR of the four samples at high (~20 T) and the now available ultrahigh 35.2 T SCH magnetic fields have paved the way for solid-state ^{95}Mo NMR as a new

https://doi.org/10.1021/acs.jpcc.0c10522
J. Phys. Chem. C 2021, 125, 7824−7838

analytical tool in the characterization of MoS_2 nanomaterials. For example, our experimental results have provided the information that the electronic band gaps of multilayered 2H-MoS_2 materials correlate with either the number of layers or T_1^{CSA} determined by NMR. Moreover, for a particular 2H-MoS_2 layer material, it is experimentally observed that the band gap, characterized by its τ_c or relative τ_c/τ_c^T values observed at three widely different B_0 fields, is not influenced by a change in the magnetic field strength B_0. Because the ^{95}Mo EFG and CSA spectral parameters determined for the four different MoS_2 samples are all identical (Table 1), that is, the local crystalline Mo environments for all four samples are identical, it is likely that the "pseudo-amorphous" (sample 2) and catalyst (sample 3) samples would have yielded corresponding results at 35.2 T as obtained for the two 2H-MoS_2 samples. It is found that the $T_1(^{95}Mo)$ spin−lattice relaxation time for the 160- and 4-layer samples shortens at high magnetic field B_0 and proportional to B_0^2. This shows that the CSA (~1025 ppm) is the dominant $T_1(^{95}Mo)$ relaxation mechanism for multilayered MoS_2 samples. The CSA mechanism suggests that the MoS_2 band gap electrons, delocalized throughout the 2H-MoS_2 lattice-layer structures, are the likely fast modulation source ($\omega_o\tau_c \ll 1$) of ^{95}Mo T_1^{CSA} relaxation similar to the field-proportional Knight shift. In addition, from the layered 2H-MoS_2 samples studied here, it is observed that $T_1(^{95}Mo)$ is lower for a few-layered compared to a high-layer MoS_2 sample, when obtained at identical B_0 magnetic field strength. This illustrates a tunable effect on the electronic band gap with the number of layers. A comparison of our $T_1(^{95}Mo)$ data in Table 4 with those reported/estimated earlier[11,13] shows that these two early studies employed multilayered MoS_2 samples with much more than 160 layers. The combination of high magnetic field strengths B_0 and short $T_1(^{95}Mo)$ relaxation times along with the above NMR pulse sequences allows acquisition of spectra for the four MoS_2 nanomaterials studied here at a reasonable time (~30 min to 24 h) for a 30 μL sample volume. In particular, we note that application of the MAS-QCPMG pulse sequence to the surface of a real HDS catalyst, that is, the MoS_2−Al_2O_3 surface of sample 3, has allowed the first example ever observed for a MAS NMR spectrum at natural-abundance for a low-γ nucleus species monolayer on a catalyst support. The striking difference in the appearance of the ^{95}Mo MAS NMR spectra for the 160- and 4-layer samples at 35.2 T with an almost complete disappearance of the 4-layer spectrum into the noise level is caused by a dispersion in the isotropic chemical shift as judged from the increased line widths for this sample with an increase in the magnetic field B_0. Finally, the results reported here for the multilayered MoS_2 samples show that while $T_1(^{95}Mo)$ decreases the MAS line width increases with a decreasing number of layers in multilayered 2H-MoS_2. This is due to an increasing distribution of the isotropic ^{95}Mo chemical shift caused by the decrease in the number of layers, that is, crumpled, rose-like, and defective Mo-edge structures. The experimental solid-state ^{95}Mo NMR results and observations presented in this study may contribute to an increased understanding of the multifunctional aspects of the important MoS_2 material in chemistry and physics.

A theoretical study on the bonding picture in the MoS_2 monolayer, entitled "σ-aromaticity in the MoS_2 monolayer", has recently been published.[1] The unusually large MoS_2 CSA (~1025 ppm) observed for all four samples in the present study appears to be related to the results of a much higher electron charge density on Mo relative to S inside the four local identical structure of the hexagonal Mo-S rings, where Mo is the main carrier of "σ-aromaticity" described.[1] This is the first ever published theoretical study related to our experimental results reported here and earlier[14] on the significant importance of ^{95}Mo CSA in MoS_2 associated with the proposed phonon-modulated CSA relaxation mechanism.

■ ASSOCIATED CONTENT

Supporting Information

The Supporting Information is available free of charge at https://pubs.acs.org/doi/10.1021/acs.jpcc.0c10522.

Band gap phonon correlation times (τ_c) for four 2H-MoS_2 samples; plots of $T_1(^{95}Mo)$ versus τ_c/τ_c^T at B_0 fields of 14.1 T, 19.6 T, and 35.2 T; and EM images and PXRD diagrams (PDF)

■ AUTHOR INFORMATION

Corresponding Author

Hans J. Jakobsen − *Department of Chemistry, Interdisciplinary Nanoscience Center (iNANO), Aarhus University, DK-8000 Aarhus C, Denmark;* orcid.org/0000-0002-9530-495X; Phone: +45 5219 2438; Email: hja@chem.au.dk; Fax: +45 8619 6199

Authors

Henrik Bildsøe − *Department of Chemistry, Interdisciplinary Nanoscience Center (iNANO), Aarhus University, DK-8000 Aarhus C, Denmark*

Martin Bondesgaard − *Department of Chemistry, Interdisciplinary Nanoscience Center (iNANO), Aarhus University, DK-8000 Aarhus C, Denmark*

Bo B. Iversen − *Department of Chemistry, Interdisciplinary Nanoscience Center (iNANO), Aarhus University, DK-8000 Aarhus C, Denmark;* orcid.org/0000-0002-4632-1024

Michael Brorson − *Haldor Topsøe A/S, DK-2800 Lyngby, Denmark*

Flemming H. Larsen − *Department of Food Science, University of Copenhagen, DK-1958 Frederiksberg C, Denmark*

Zhehong Gan − *National High Magnetic Field Laboratory, Tallahassee, Florida 32310, United States;* orcid.org/0000-0002-9855-5113

Ivan Hung − *National High Magnetic Field Laboratory, Tallahassee, Florida 32310, United States;* orcid.org/0000-0001-8916-739X

Complete contact information is available at: https://pubs.acs.org/10.1021/acs.jpcc.0c10522

Notes

The authors declare no competing financial interest.

■ ACKNOWLEDGMENTS

This work is a result of a collaborative research between Aarhus University and the National High Magnetic Field Lab (NHMFL or MagLab), Florida State University (FSU), Tallahassee, where H.J.J. was a visiting professor during the period 2012−2017. The present work was supported by the Danish National Research Foundation (H.J.J., early stage 1995−2010, and B.B.I., DNRF93), the Villum Foundation, Haldor Topsøe A/S, and by the Department of Chemistry, Aarhus University. The MoS_2 samples were synthesized at

Haldor Topsøe A/S and at Aarhus University, except for the original 160-layer sample (which was kindly provided by Prof. K. Schaumburg, Roskilde University, Denmark). All samples were characterized by TEM or STEM at Aarhus University. The high (19.6 T) and ultrahigh (35.2 T) magnetic field NMR experiments in this work were all performed at the National High Magnetic Field Laboratory, which is supported by the National Science Foundation Cooperative Agreement DMR-1644779 and the State of Florida. Development of the 36 T SCH magnet and NMR instrumentation were supported by NSF (DMR-1039938 and DMR-0603042) and NIH (BTRR 1P41 GM122698).

REFERENCES

(1) Kulichenko, M.; Boldyrev, A. I. σ-Aromaticity in the MoS_2 Monolayer. *J. Phys. Chem. C* **2020**, *124*, 6267−6273. . This most recent article contains a list of 78 references related to research on MoS2 performed during the past two decades

(2) Bronsema, K. D.; De Boer, J. L.; Jellinek, F. On the Structure of Molybdenum Diselenide and Disulfide. *Z. Anorg. Allg. Chem.* **1986**, *540*, 15−17.

(3) Stiefel, E. I. Transition Metal Sulphur Chemistry: Biological and Industrial Significance and Key Trends. In *Transition Metal Sulphur Chemistry, Biological and Industrial Significance*; Stiefel, E. I., Matsumoto, K., Eds.; ACS Symposium Series; American Chemical Society: Washington DC, 1996; Vol. *653*, Chapter 1, pp 2−38.

(4) Novoselov, K. S.; Geim, K. S.; Morozov, S. V.; Jiang, D.; Zhang, Y.; Dubonos, S. V.; Grigorieva, I. V.; Firsov, A. A. Electric Field Effect in Atomically Thin Carbon Films. *Science* **2004**, *306*, 666−669.

(5) Rase, H. F. *Handbook of Commercial Heterogeneous Catalyst*; CRC Press: Baca Raton, London, New York, Washington DC, 2000.

(6) *Synthesis of Solid Catalysts*; De Jong, K. P., Ed.; Wiley-VCH: Weinheim, 2009.

(7) Topsøe, H.; Clausen, B. S.; Massoth, F. E. Hydrotreating Catalysis. In *Catalysis—Science and Technology*; Anderson, J. R., Boudart, M., Eds.; Springer: Berlin, 1996; Vol. *11*, pp 1−310.

(8) Wang, C. Progress in Electrocatalytic Hydrogen Evolution Based on Monolayer Molybdenum Disulfide. *Front. Chem.* **2019**, *7*, 131.

(9) Besenbacher, F.; Brorson, M.; Clausen, B. S.; Helveg, S.; Hinnemann, B.; Kibsgaard, J.; Lauritsen, J. V.; Moses, P. G.; Nørskov, J. K.; Topsøe, H. Recent STM, DFT, and HAADF-STEM Studies of Sulfide Based Hydrotreating Catalysts: Insight into Mechanistic, Structural and Particle Size Effects. *Catal. Today* **2008**, *130*, 86−96. and references cited therein

(10) Edwards, J. C.; Ellis, P. D. Solid-State ^{95}Mo NMR Study of Hydrodesulfurization Catalysts. 2. Investigation of Reduced/Sulfided Molybdena-Alumina Catalysts and the Effect of Promotor Ions on "Fresh" and Reduced/Sulfided Molybdena-Alumina Catalysts. *Langmuir* **1991**, *7*, 2117−2134. . See also references cited therein

(11) Bastow, T. J. ^{95}Mo NMR: MoO_3, MoS_2, $MoSe_2$, Mo_3Se_4, $MoSi_2$ and Mo_2C. *Solid State Nucl. Magn. Reson.* **1998**, *12*, 191−199.

(12) de Lacaillerie, J.-B. d.; Gan, Z. MAS NMR Strategies for the Characterization of Supported Molybdenum Catalysts. *Appl. Magn. Reson.* **2007**, *32*, 499−510.

(13) Panich, A. M.; Shames, A. I.; Rosentsveig, R.; Tenne, R. A Magnetic Resonance Study of MoS_2 Fullerene-Like Nanoparticles. *J. Phys.: Condens. Matter* **2009**, *21*, 395301.

(14) Jakobsen, H. J.; Bildsøe, H.; Skibsted, J.; Brorson, M.; Schaumburg, K. Natural Abundance Solid-State ^{95}Mo MAS NMR of MoS_2 Reveals Precise ^{95}Mo Anisotropic Parameters from Its Central and Satellite Transitions. *Chem. Commun.* **2010**, *46*, 2103−2105.

(15) Skibsted, J.; Nielsen, N. C.; Bildsøe, H.; Jakobsen, H. J. ^{51}V MAS NMR Spectroscopy: Determination of Quadrupole and Anisotropic Shielding Tensors, Including the Relative Orientation of their Principal-Axis Systems. *Chem. Phys. Lett.* **1992**, *188*, 405−412.

(16) Jakobsen, H. J.; Bildsøe, H.; Skibsted, J.; Giavani, T. ^{14}N MAS NMR Spectroscopy: the Nitrate Ion. *J. Am. Chem. Soc.* **2001**, *123*, 5098−5099.

(17) Giavani, T.; Bildsøe, H.; Skibsted, J.; Jakobsen, H. J. Determination of Nitrogen Chemical Shift Anisotropy from the Second-Order Cross-Term in ^{14}N MAS NMR Spectroscopy. *Chem. Phys. Lett.* **2003**, *377*, 426−432.

(18) Gan, Z.; Hung, I.; Wang, X.; Paulino, J.; Wu, G.; Litvak, I. M.; Gor'kov, P. L.; Brey, W. W.; Lendi, P.; Schiano, J. L.; et al. NMR Spectroscopy Up to 35.2 T Using a Series-Connected Hybrid Magnet. *J. Magn. Reson.* **2017**, *284*, 125−136.

(19) Larsen, F. H.; Jakobsen, H. J.; Ellis, P. D.; Nielsen, N. C. Sensitivity-Enhanced Quadrupolar-Echo NMR of Half-Integer Quadrupolar Nuclei. Magnitudes and Relative Orientation of Chemical Shielding and Quadrupolar Coupling Tensors. *J. Phys. Chem. A* **1997**, *101*, 8597−8606.

(20) Larsen, F. H.; Jakobsen, H. J.; Ellis, P. D.; Nielsen, N. C. QCPMG-MAS NMR of Half-Integer Quadrupolar Nuclei. *J. Magn. Reson.* **1998**, *131*, 144−147.

(21) Larsen, F. H.; Jakobsen, H. J.; Ellis, P. D.; Nielsen, N. C. High-Field QCPMG-MAS NMR of Half-Integer Quadrupolar Nuclei With Large Quadrupole Couplings. *Mol. Phys.* **1998**, *95*, 1185−1195. and references cited therein

(22) Weber, M. J. Temperature Dependence of Spin-Lattice Relaxation in Alkali Halides. *Phys. Rev.* **1983**, *130*, 1−10.

(23) Chianelli, R. R.; Prestridge, E. B.; Pecoraro, T. A.; DeNeufville, J. P. Molybdenum Disulfide in the Poorly Crystalline "Rag" Structure. *Science* **1979**, *203*, 1105−1107.

(24) Harris, R. K.; Becker, E. D.; Cabral de Menezes, S. M.; Goodfellow, R.; Granger, P. NMR Nomenclature. Nuclear Spin Properties and Conventions for Chemical Shifts. *Pure Appl. Chem.* **2001**, *73*, 1795−1818.

(25) Bildsøe, H. *Varian Manual, STARS (SpecTrum Analysis of Rotating Solids) User's Guide*. Publication No 87-195233-00, Rev. A0296, 1996. Based on Jakobsen, H. J.; Skibsted, J.; Bildsøe, H.; Nielsen, N. C. Magic-angle spinning NMR spectra of satellite transitions for quadrupolar nuclei in solids. J. Magn. Reson. 1989, 85, 173−180.

(26) Jakobsen, H. J.; Hove, A. R.; Bildsøe, H.; Skibsted, J.; Brorson, M. Long-Term Stability of Rotor-Controlled MAS Frequencies to 0.1 Hz Proved by ^{14}N MAS NMR Experiments and Simulations. *J. Magn. Reson.* **2007**, *185*, 159−163.

https://doi.org/10.1021/acs.jpcc.0c10522
J. Phys. Chem. C 2021, 125, 7824−7838